MASTER THESIS

SAFETY ASSESSMENT OF RUNNING WITH A BONE-ANCHORED PROSTHESIS IN A PERSON WITH A TRANSTIBIAL AMPUTATION; A PILOT STUDY

Marnick Los

FACULTY OF ENGINEERING TECHNOLOGY
DEPARTMENT OF BIOMECHANICAL ENGINEERING

EXAMINATION COMMITTEE
Prof. Dr. Ir. N.J.J. Verdonschot
Dr. Ir. M. Asseln
Dr. R.A. Leijendekkers
Dr. E.C. Prinsen
Dr. Ir. P. Tzanetis

27-06-2024

UNIVERSITY OF TWENTE.

Orthopaedic Research Laboratory
Radboudumc

General introduction

Lower limb amputations, often a consequence of conditions such as diabetes, peripheral vascular disease, trauma, and infections, substantially impact the mobility and quality of life of affected individuals [1]. The incidence and cause of lower limb amputations vary globally, with significantly higher rates observed in populations at risk for Diabetes Mellitus [2]. However, the number of trauma related amputations is also substantial with an estimated prevalence of over 55 million worldwide [3].

Incidence of transtibial amputations in the Netherlands is estimated at 1260 each year on average over the period of 2012-2021 [4]. Using the average Dutch population over this period [5], an estimated incidence rate of 7.4 per 100.000 can be computed. A series of studies [6,7] conducted in the north of the Netherlands reported an incidence rate of 9.9 new amputations for each 100.000 inhabitants per year for the period of 2012-2013, which is a slight increase over the 8.8 over 2003-2004 which was unchanged since 1991-1992. Assuming this steady rate, a substantial population of amputees require rehabilitation and medical devices to regain mobility.

Figure 1: Illustrations of a transtibial socket suspended prosthesis (left) and a bone anchored prosthesis (right).

A socket-suspended prostheses is a common solution for amputees to restore mobility and facilitate return to daily life after amputation. These prostheses are designed to fit the residual limb tightly on an intermediate liner around the skin of the stump. The prosthesis is suspended below the socket and load is transmitted from the prosthesis to the body via the socket, liner, skin, and residual soft tissue. Applying loads on the skin causes problems for many amputees, a study by Meulenbelt et al. reported an incidence rate for skin issues of 63% in one month for lower limb amputees, a different Dutch study by Dudek et al. [8] reported a prevalence of 40.7% among lower limb amputees. They categorised issues and attributed causes by the socket to Eczema, mechanical and occlusion. The stress and shear on the skin in combination with a humid environment within the socket leads to skin problems such as erythema and oedema [8]. These skin conditions can be immobilising for a lower limb amputee as the treatment often requires offloading of the stump, rendering the prosthesis unusable [9]. Quality of life is associated with an individual's mobility and independence, which relies on the ability to use a prosthetic aid [10], driving the development of solutions or alternatives to avoid skin problems. Many developments have been made to improve the comfort and the socket fit, but for some amputees these problems remain unresolved [11,12].

A bone-anchored prosthesis (BAP) could provide a solution for amputees that experience (chronic) skin problems. A BAP relies on the principle of osseointegration, which is the process of direct structural fixation of an implant in living bone [13]. After development of implants using osseointegration for various dental and orthopaedic applications, the bone anchored prosthesis was introduced for a transfemoral amputee in 1990 [13,14]. This application has since then been further developed and various different designs of implants have been used in clinical practice [15]. Performance of femoral implants has improved over time and positive outcomes encouraged the development of BAPs for transtibial amputees which are now also clinically available [16].

Due to the relatively young nature of BAPs, much is unknown about the biomechanics of osseointegrations in this application. The strength of the bone-implant interface of implants used for BAPs and its resilience to cyclic loading during gait has not been measured of simulated and validated. Much knowledge can be obtained from the field of total joint replacements of the hip and knee, but both are different. Histological retrieval studies [17–19] have reported complete ingrowth and adherence of the bone on implant surface and densification of bone tissue in contact for transfemoral osseointegration implants, which implies a stable connection at bone-implant interface, however bone resorption at the distal end of this type of implants have also been reported [15,17,20,21]. The effect of periprosthetic bone resorption has been studied extensively for total hip replacement implants and attributed to the lack of loading due to stress shielding by the implant[22]. This effect has not yet been researched for transtibial bone anchored prostheses [23,24], but should be considered in a biomechanical evaluation of transtibial bone anchored prosthesis.

It should be noted that the transtibial osseointegration implant is fundamentally different from the transfemoral implant. The transtibial implant resides in the metaphysis of the tibia with its proximal tip already at the transition of meta- to epiphysis where load is transferred from the implant to the tibia through trabecular bone. The femoral implant is located in the diaphysis of the femur and is enveloped mostly by cortical bone [17]. This discrepancy can have significant effects on bone remodelling and how the implant interface transfers load to the bone.

Clinical follow up studies [25,26] report positive outcomes of transtibial bone anchored prostheses. Mechanical failures of bone anchored prostheses are rare but do occur[27]. Known mechanical failure modes of the system are periprosthetic fractures, device breakage, and (a)septic implant loosening, which are mostly observed in transfemoral implants[27]. Adverse events of non-mechanical nature like infections of the stoma at the site of the implant protrusion and septic loosening are also known risks of osseointegration implants. Adverse event of transtibial bone anchored protheses are underreported [27], resulting in only a limited perspective of the possible failures. Reported adverse events of transtibial BAPs consist of breakages of the dual cone adapter that connects the intramedullary implant to external components [27].

There is a large interest in the limitations of activities among BAP users. Due to the high associated risks with mechanical failure, allowed sport activities prescribed by clinicians are generally conservative. However, mechanical limits of the osseointegrated system remain mostly unknown. For the potential mental and physical health benefits of sport, it is worth investigating the safety of performing sports on a BAP. The risks of mechanical failure of the bone implant system also affects the acceptance of BAPs among prosthesis users. Beside the risk of infection, the second most perceived disadvantage among amputees considering a BAP, is the potential for limited activity due to risk of implant failure [28]. Reported patient considerations are 'risk of bone fracture', 'bent or broken implant' and 'need to avoid running' [28].

Gaining knowledge of the biomechanics of running on a bone anchored prosthesis provides insights into the risk of mechanical failure of a transtibial BAP but presents both methodological and ethical challenges. Running is not known to be safe for a BAP, obtaining experimental data is inherently not free of risk and data from able bodied persons is invalid for the modelling of amputee motion as there are substantial differences in able bodied and amputee kinematics [29]. An earlier study by Thesleff et al. [30] investigated running on a transfemoral implant by using kinetics and kinematics from an able-bodied dataset on a musculoskeletal model adjusted for a BAP. This provides an indication of loads applied on the implant, but this does not respect amputee gait and limits for safe loads were obtained using synthetic femora. No similar studies were found for transtibial amputees. Some studies [31,32] reported forces and moments along the length of the tibia during activities of daily life including walking, but not considering running. Overall, maximal allowable load values for forces and moments acting on the implant are not known, and a single value would not represent the complex connection of osseointegration.

A comprehensive overview of efforts made to characterise the bone-implant system for femoral BAPs using a variety of ex vivo and in silico models is reported by Galteri et al. [33]. Different finite element (FE) models were developed to study load transfer from the implant to bone in a femoral bone anchored prosthesis. Knowledge from in vitro and in silico studies require validation, but as osseointegration can only be achieved in vivo, validation of the implant bone interface in models remains a challenge. Models used to predict periprosthetic bone stress make assumptions about the contact interaction [33]. Also the used material models for bone tissue vary among studies [33]. Only two FE models were found that performed a validation of their FE model for the modelling of stress/strain in periprosthetic bone [33–35], which used cortical strain and displacement of ex vivo models.

The aim of this case study is to investigate the safety of running on a BAP for a single person with a transtibial amputation by using experimental data and FE modelling to assess risk of mechanical failure. Experiments were performed in the gait lab of the Radboud medical centre, where kinematics and ground reaction forces were recorded of a transtibial amputee who performed walking and running trials. The forces and moments on the implant are computed for different conditions using multi body models with inverse dynamics. A FE model was created of the tibia and implant to compute local stresses and stress/strength ratio in the bone model to evaluate the risk of local bone fractures. This type of model and simulations are subject to assumptions and validation was not available. Therefore, the results of running trials were compared to walking trials, such that a risk of failure during running can be related to walking, which is assumed to be safe from practice.

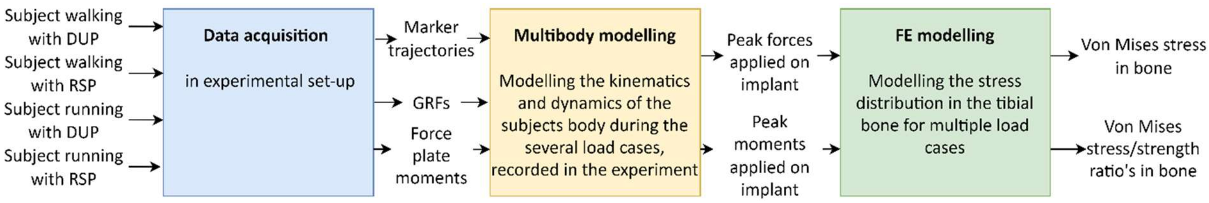

Figure 2: Global flow phases and transfer of data in this project.

In the project separate phases can be defined as shown in Figure 2, an experimental, multibody modelling and FE modelling phase. This report is divided in two separate sections in pap format. The first section describes the development of a multibody model for processing the motion capture data and ground reaction forces to external forces and moments applied on the implant. The second section describes the development of a personalised FE model to analyse the transmission of forces and moments of the implant on the bone and the distribution of stress and ratio of stress/strength to assess local risk of fracture and assess the question whether it is safe to run with a transtibial BAP.

Contents

Section 1: Implant load during running on a transtibial bone anchored prosthesis, a multibody modelling approach

Keywords: bone anchored prosthesis; Multibody modelling; running; Osseo integrated implant; transtibial amputation; implant loading; Dual cone loading; gait analysis; motion capture

Abstract

Bone anchored prosthesis (BAP) is a promising approach for transtibial amputees to enable a direct load transfer and prevent socket-related problems. However, it is unknown if high load/ dynamic activities, such as running, is safe. Mechanical failure of the implant or bone could lead to fractures resulting in dangerous situations for the amputee following trauma surgery interventions and explantation of the device. In the recent years, osseointegrated implants for BAPs performed well in walking, but limits of mechanical loads are unknown. The aim of this study was to determine the loads acting on the implant during running versus walking, the effect of a running specific prosthesis (RSP) versus a Daily use prosthesis (DUP), and the speed of running. Experimental gait data was obtained for a unilateral transtibial amputee with a bone anchored prosthesis. Experiments were performed for walking and running on a DUP and a RSP. Two multi body models of the participant with either prosthesis were constructed to express the local forces and moments acting on the implant and dual cone adapter in a local reference frame. It was found that local forces in the transverse plane and bending moments about AP and ML axes were smaller during running compared to walking, but axial compression forces were higher for running. Temporal load distribution was different between DUP and RSP, but magnitudes were similar. The effect of increasing running speed did not increase localised implant loads significantly, it resulted in an increased ground reaction force for the intact limb, but effect on the prosthesis side was minimal.

1. Introduction

The bone-anchored prosthesis (BAP) is an alternative for the socket suspended prosthesis (SSP) and relies on the concept of osseointegration to achieve a rigid fixation between an implant and the intramedullary cavity of a long bone.

Despite all the development on socket-suspended prosthesis on comfort, skin related problems remain a very prevalent issue [8,9,11,12]. The bone-anchored prosthesis (BAP) avoids loading of the skin, circumventing skin related issues, such as erythema and oedema, caused by the pressure of a socket. The BAP has shown to be a promising alternative for amputees with socket related problems [36]. An additional advantage of the BAP is the sensation of direct load transfer from the prosthetic to the bone. This phenomenon is referred to as osseoperception [37].

The intracorporeal components consists of an intramedullary implant with a porous coating, or other surface structure that promotes bone ingrowth and an adapter with two morse tapers on both ends referred to as dual-cone adapter (DCA). The implant is also optionally fixed with transverse screws. The proximal end of the DCA inserts in the implant and connects to an extracorporeal prosthesis distally. The DCA is secured with a screw that extends through the hollow DCA and engages thread in the implant and presses the screwhead on the DCA internally.

There are two shear pins on the proximal end of the DCA that are designed to break in case of excessive torsional loads which protects the bone implant interface [15]. Additionally, a torque limit safety mechanism is also included in the connector that connects the DCA to the external part of the prosthesis. The DCA itself can also be seen as a failsafe mechanism that will theoretically break before the implant-bone system in case of excessive loads.

Despite the advantages and low incidence of mechanical failures of the BAP, complications associated with adverse events regarding BAP are more severe compared to a SSP. Known major risks of the BAP observed in transfemoral implants are device breakage, implant infection and implant loosening [27]. Atallah et al. [27] reported that peri-prosthetic fractures occurred only in transfemoral amputees and were the result of falling. Adverse events of transtibial BAP are underreported, the only device failures mentioned are device breakages of the dual cone adapter [27].

High bending moments during falls are identified as the critical loading conditions for bone fracture and device breakage for the bone-implant system [33,38]. Aseptic loosening is a result of excessive micromotions [33]. This is hypothesised to be the result of high shear and tensile stresses at the bone implant interface. Shear stress tangent to the bone-implant interface results from axial compression and torsion about the longitudinal axis. Interface tensile stress at the distal tibia is the result of bending moments and forces in a transverse plane.

Beside these major adverse events, stoma infection is a more prevalent issue, but is not associated with mechanical failure. These risks also affect the acceptance of BAPs among prosthesis users. Beside risk of infection, the second most perceived disadvantage among amputees considering a BAP is the potential for limited activity due to risk of failure [28]. Patients indicate their considerations are ‘risk of bone fracture’, ‘bent or broken implant’ and ‘need to avoid running’ [28].

There is a large interest among BAP users in the limitations of activities. Due to the suggested high associated risks with an adverse event, limitations on sport activities prescribed by clinicians are generally conservative. However, mechanical limits of the osseointegrated system remain mostly unknown, obtaining a better knowledge of the mechanical limits of the system might result in the ability of BAP users to perform sport activities.

A better understanding and quantification of the loads on the implant and bone provides insights in the risk of mechanical failure of a transtibial BAP.

In healthy feet the ankle joint stiffness is modulated during gait by muscle co-contraction[39]. This stiffness is modulated to absorb and release energy effectively during both walking and running. Common passive carbon prosthetic feet are designed for activities of daily living and their stiffness is tuned for effective walking gait and not for running. Active SSP users are able to run and perform sport at paralympic levels on running specific prostheses (RSP) constructed with a carbon fibre blade. RSPs are designed for amputees to improve performance in running by storing energy in the blade during absorption phase and release energy during the propulsion phase [40]. The resulting gait pattern better resembles a healthy runner and leads to a more symmetric gait pattern [41]. The compliance of the blade in the RSP might also be able to improve temporal load distribution which would reduce peak load on the implant. It is therefore interesting to investigate the effect of these different types of prosthesis on the implant load as this might affect.

This study is aimed to explore for the first time the differences in load between walking and running, for an amputee with a transtibial BAP. So, in this study, forces and moments are determined that act on an osseointegration implant for a BAP during walking and running (at varying speeds) on both a DUP and RSP. Loads are compared to the load during level walking for reference, which is assumed to be safe for walking based on practice.

2. Materials & Methods

2.1 Subject & instrumentation

One female participant (body mass: 67 kg, body height: 168 cm) with a left-sided unilateral transtibial amputation volunteered and participated in this study under informed consent. The participant had received a personalised BADAL X® OTI (OTN implants B.V.) more than 3 years prior to the experiment and was comfortable with walking on her daily prosthesis. Her DUP consists of a GV20 connector, conventional tube and alignment components and a PRO-FLEX® LP ALIGN foot in a neutral running shoe. A RSP was built by connecting the GV20 to a FLEX-RUN™ JUNIOR FSX0076 blade. The RSP was constructed with conventional components and fitted and aligned for the participant prior to the experiment, this moment was the only prior experience of the participant with using a RSP. Both prostheses are illustrated in Figure 3.

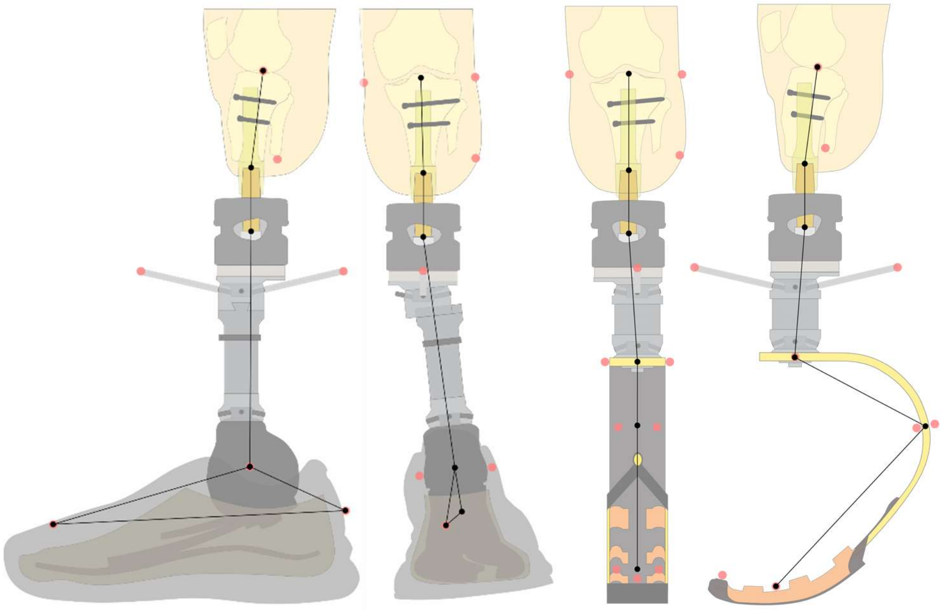

Figure 3: Schematic illustration of construction of segments based on prosthesis geometry and residual limb anatomy. Red dots represent markers and black dots and lines represent model segments. The black connector is illustrated with a see through to visualise the distal end of the DCA.

2.2 Data acquisition & pre-processing

In the morning of the experimental day the participant accommodated to the RSP and the alignment of the RSP was optimised by the certified prosthetist and orthotist. In the afternoon the participant was equipped with reflective markers and trials were recorded of skipping in place, walking at a self-selected comfortable walking speed (CWS) 4.75 km/h and 5.5 km/h for both DUP and RSP, however walking at CWS on RSP was performed on a single belt resulting making the measurement unusable. Running trials were performed iteratively faster within a comfortable range with sufficient rest between trials. Resulting in trials on DUP for 6.5 and 7.0 km/h and for RSP at 6.5, 7.0, 7.5 and 8.0 km/h.

For each trial, treadmill speed was increased gradually, and recordings started when the target speed is reached and ended after approximately 20 valid strides were achieved for each side.

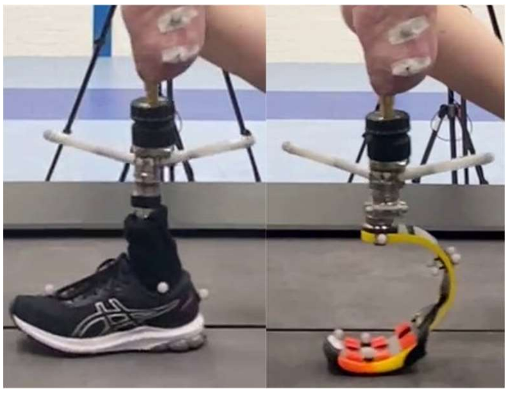

Figure 4: Images of a daily use prosthesis (DUP; left) and a running specific prosthesis (RSP; right) with applied markers.

Trials were performed on an instrumented split belt treadmill (Motek Medical B.V) outfitted with two force plates, both recording force and moments about three axes on the plate at 2000 Hz. Walking trials were performed using both belts. Running trials were performed on a single belt to prevent crosstalk during strides on the edge between the belts. A synchronised VICON camera system (Vicon Motion Systems Ltd) recorded marker trajectories at 100Hz. For the kinematics, the full body plug in gait model by VICON [42] was used with modification for the lower prosthetic limb. Two markers were attached to the pyramid adapter below the GV20 connector similar to a previous study by Jonkergouw et al. [43], and markers were placed on the DUP at positions similar to anatomical landmarks. The markers for the RSP were placed at top, bottom, and apex of the blade (Figure 3). Using the VICON NEXUS suite, marker data was labelled, gap filled and filtered using a Woltring filter (quintic spline) with Mean Squared Error of 10.

All further processing and modelling was performed in MATLAB. The ground reaction forces (GRFs) were filtered using a zero-lag second order low-pass Butterworth filter with 10 Hz cut-off frequency. Centre of pressure (COP) was determined as (dx, dy) from the GRFs and moments on the force plates using the following equations:

$$Mx = Fz * dy + Fy * dz$$
$$My = Fz * dx + Fx * dz$$

Heel strike (HS) and toe-off (TO) events were detected using the jerk of vertical GRF and thresholding at 20N. For the running trials ran on a single belt, the GRFs were separated for left and right in between the TO and subsequent HS.

2.3 Multibody modelling

To compute loads of the transtibial BAP, an anthropometric multibody model with inverse dynamics functionality [44] developed at the VU Amsterdam [45] was used and modified to accommodate for both a DUP and RSP (Figure 3 and Figure 5). The original model [46] uses anthropomorphic data to define inertial properties for segments representing anatomical bodies. Prosthetic model segments were constructed respecting the geometry and joint/connection locations of the prosthesis as illustrated in Figure 3. Inertial parameters of the prosthetic segments were determined by combining inertial properties of individual prosthetic components as point masses.

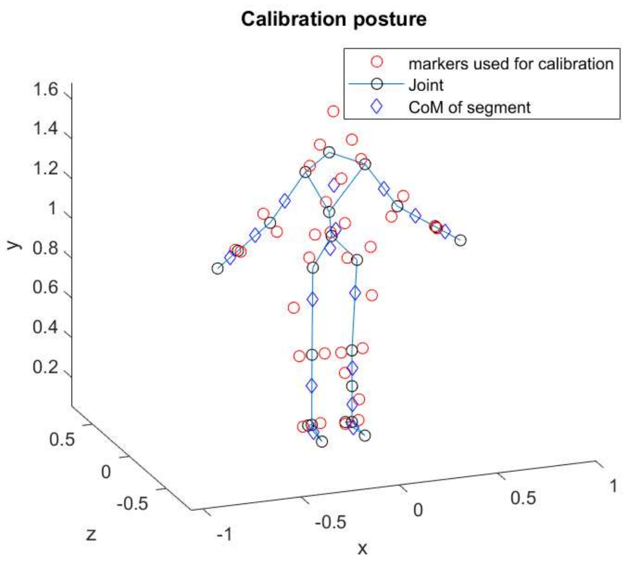

Figure 5: Visualisation of the model in a static trial for the DUP with annotated segments, joints, centre of masses (COMs) and markers.

A schematic of the data flow for the model is presented in Figure 7. The model computes forces and moments expressed in a global coordinate system. To express loads in the implant reference frame, a coordinate transformation was applied using the dynamic orientation of the DCA illustrated in Figure 3. The distal DCA location is defined combining the location of the pyramid adapter with the offset known from the components. The y-axis of the implant reference frame (Figure 6) is aligned with the mediolateral (ML) axis defined by knee markers, z-axis is defined from the distal DCA to the knee joint centre, and the x-axis is aligned in anterior-posterior (AP) direction and was calculated using the cross product. Joint forces and moments were obtained within this reference frame using inverse dynamics for the stance phase defined from heel strike (HS) to toe-off (TO).

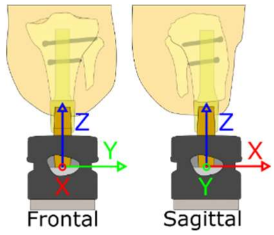

Figure 6: Schematic representation of implant reference frame in which loads are expressed. Y-axis is aligned with the ML knee joint. Z-axis is aligned with the longitudinal axis aimed proximally; x-axis is aimed anteriorly.

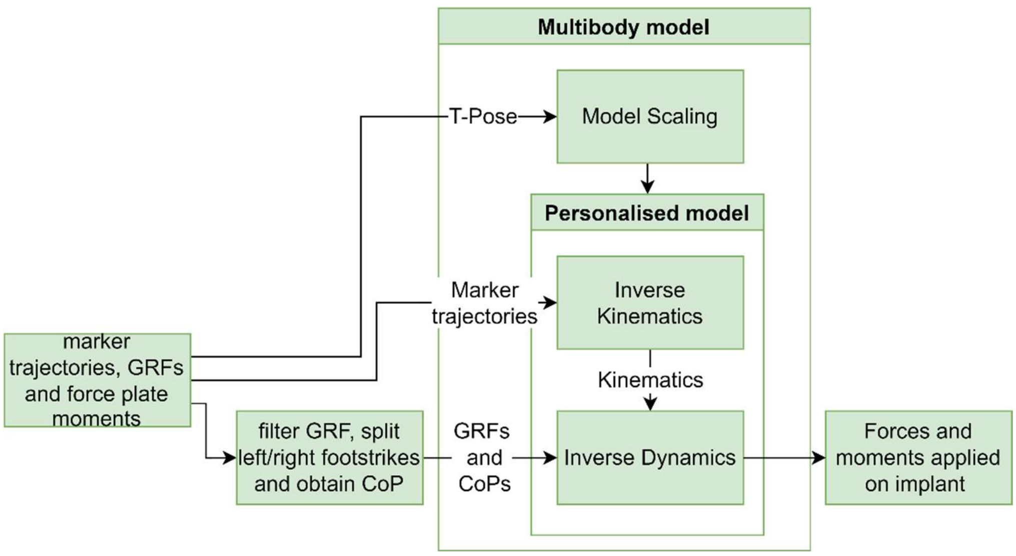

Figure 7: Schematic description of global steps applied for processing raw ground reaction forces and marker trajectories to forces and moments.

2.4 Post-processing and statistical analysis

For all trials, vertical GRFs were assessed for crosstalk between the force plates, invalid strides were excluded from further analysis. Crosstalk was identified where the GRF was nonzero during swing phase, for example the three strides between samples 1400 and 1700 in Figure 8. Strides were also excluded when crosstalk affected the detecting of TO as visible in the left stride near sample 2600 in Figure 8.

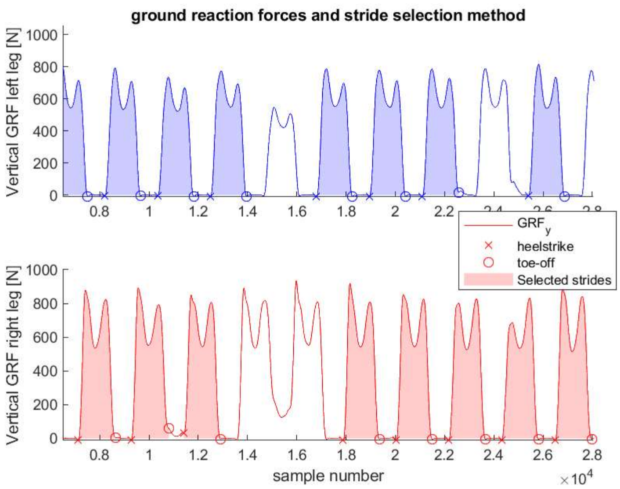

Figure 8 Vertical ground reaction forces of a walking trial with annotated HS and TO. Shaded areas under the curve indicate a valid stride selected for further processing. Unshaded strides are excluded due to crosstalk or invalid HS

All valid strides for a trial were normalised from HS to TO and interpolated using a Piecewise Cubic Hermite Interpolating Polynomial (PCHIP) method to obtain an equal number of samples for each stride while conservatively preserving the shape of the curve. Ensemble averages and standard deviations were computed from normalised strides to obtain average forces and moments for the full stance phase with a standard deviation between strides.

The stance phase is defined from HS to TO, where midstance is found at the local minimum of vertical GRF at ~50% stance in walking and at the peak vertical GRF ~40% of stance during running. The phase from HS to midstance is referred to as the absorption phase and midstance to TO as the propulsion phase (Figure 9).

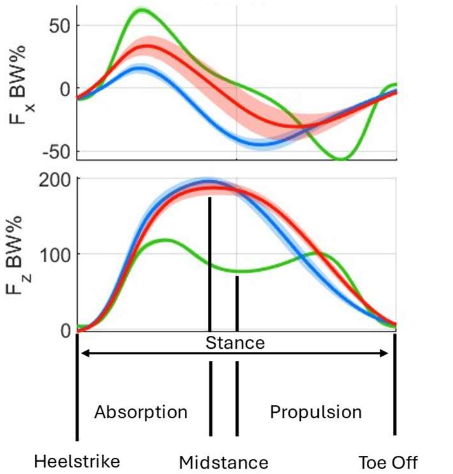

Figure 9: Example of AP and vertical forces during stance and definition of gait events and phases. Midstance is defined as the local minimum during walking gait (green), and as maximum during running (red:RSP/blue:DUP).

To normalise results forces are expressed as a percentage of bodyweight and moments as a percentage of body weight multiplied by bodyheight [31]. Temporal distributions of forces and moments over the stance phase are presented as a mean with a single standard deviation among strides as a shaded area.

Peak loads are determined during walking for both the absorption and propulsion phases by extracting forces and moments at the peak AP force. For running, peak loads are also determined for both absorption and propulsion phases as AP forces and bending moments are highest here, but also peak loads during midstance was determined as this contained the highest vertical force.

3. Results

In Figure 10 the temporal load distributions for walking on the DUP and running on both DUP and RSP are presented for comparison. Peak loads are presented in Table 1 and Table 2 for walking and running respectively.

Peak forces in AP direction are larger during walking compared to running for both DUP and RSP. During the absorption phase, peak AP force of running on the RSP was 47% of the force recorded during walking. For the DUP this was 26%. During propulsion, peak AP force during running was 87% and 72% of walking for DUP and RSP respectively. Stride duration was much shorter during running compared to walking, with 0.30 and 0.32 seconds for running on DUP and RSP respectively and 0.69 and 0.64 during walking for DUP and RSP respectively. Moments about the ML axis is larger during the absorption phase in walking compared to running. ML Moments during the propulsion phase for walking are similar to running on the RSP, but higher compared to running on DUP. ML forces follow a different temporal distribution for all walking and running on both DUP and RSP. Peak force is similar for DUP walking and RSP running, but RSP running standard deviation is larger. Mean and peak force during DUP running is higher compared to both walking and running on RSP. The vertical force during running is substantially larger and compared to walking for both prosthetic conditions, the peak vertical force during running was 184% and 176% of the peak during walking. During the absorption phase for running a positive moment is observed about the AP axis which is different from walking.

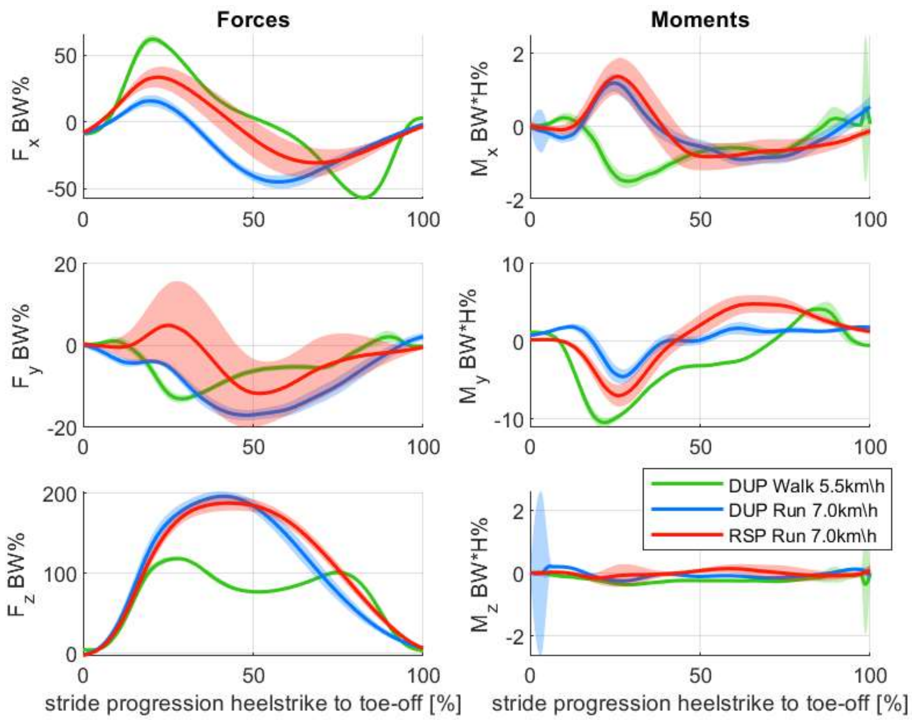

Figure 10: Mean local forces and moments during walking and running conditions from HS to TO. Shaded area represents a single standard deviation determined from individual strides.

Running on DUP versus RSP

Differences in loads during running between the DUP and RSP are small in general. Force in AP direction for the DUP was more negative compared to the RSP. Forces in ML direction are lower in the RSP compared to the DUP, but variance was much higher for the RSP compared to the DUP. Peak vertical force is slightly higher for DUP compared to RSP. Axial force during the propulsion phase is higher for the RSP compared to DUP.

Moments about the AP axis are not different between DUP and RSP. The moments about the ML axis are higher for the RSP during both the absorption and propulsion phases compared to the DUP. The moment about the ML axis for the DUP during the propulsion phase remains constant after midstance while a positive moment was recorded for the ML moment for the RSP. Moments about the vertical axis are small. A high variance is observed during the first samples, which is identified as an artefact.

Table 1 Mean (SD) peak loads for walking trials expressed in local frame, forces normalised as percentage of bodyweight and moments as percentage of body weight multiplied by bodyheight. N incicates the number of valid strides at T the average duration of the strides from HS to TO.

Prosthesis	**Speed**	**n**	**T**	**Absorption**			**Propulsion**		
				Fx/AP	**Fy/ML**	**Fz/Vert**	**Fx/AP**	**Fy/ML**	**Fz/Vert**
DUP	4.75	30	0.72	49.32(2.70)	-6.35(1.21)	97.47(4.76)	-51.22(1.69)	-1.54(1.26)	86.76(3.47)
	5.5	20	0.69	62.13(3.09)	-6.38(1.40)	106.81(4.73)	-51.22 (1.62)	-0.38(0.88)	83.41(2.32)
RSP	5.5	11	0.64	72.53(3.65)	-3.43(1.52)	96.65(4.39)	-48.72(1.34)	3.13(1.38)	73.16(3.60)
				Mx/AP	**My/ML**	**Mz/vert**	**Mx/AP**	**My/ML**	**Mz/vert**
DUP	4.75	30	0.72	-0.66(0.26)	-8.01(0.57)	-0.18(0.05)	-0.38(0.23)	2.82(0.40)	-0.20(0.12)
	5.5	20	0.69	-0.63(0.24)	-10.28(0.68)	-0.23(0.05)	-0.22(0.13)	4.05(0.28)	-0.15(0.07)
RSP	5.5	11	0.64	-0.13(0.33)	-16.77(0.85)	-0.55(0.10)	-0.05(0.19)	7.09(0.28)	-0.36(0.05)

Table 2 Mean (SD) peak forces and moments for running trials expressed in local frame, forces normalised as percentage of bodyweight and moments as percentage of bodyweight multiplied by bodyheight. N incicates the number of valid strides at T the average duration of the strides from HS to TO.

Prosthesis	**Speed**	**n**	**T**	**Absorption**			**Midstance**			**Propulsion**		
				Fx/AP	**Fy/ML**	**Fz/vert**	**Fx/AP**	**Fy/ML**	**Fz/vert**	**Fx/AP**	**Fy/ML**	**Fz/vert**
DUP	6.5	27	0.33	25.56 (5.11)	-2.59 (1.23)	152.98 (11.51)	4.09 (5.44)	-13.92 (1.60)	192.92 (8.15)	-30.28 (0.11)	-14.75 (0.63)	138.14 (0.05)
	7	29	0.32	15.86 (4.19)	-3.90 (0.60)	132.13 (12.07)	-24.43 (3.54)	-15.95 (1.48)	196.41 (5.92)	-44.76 (0.16)	-16.12 (0.67)	158.25 (0.05)
RSP	6.5	32	0.33	32.63 (5.78)	-1.50 (1.60)	138.51 (9.90)	7.60 (6.85)	-14.37 (2.23)	176.85 (6.94)	-28.47 (0.18)	-11.01 (0.78)	126.14 (0.05)
	7	26	0.30	29.36 (5.83)	-2.63 (1.64)	136.18 (8.63)	-3.93 (7.29)	-14.31 (1.97)	187.94 (9.63)	-36.72 (0.25)	-13.12 (1.09)	141.27 (0.08)
	7.5	27	0.29	32.35 (7.75)	-1.83 (1.87)	141.51 (11.75)	-0.62 (8.13)	-12.21 (2.39)	195.09 (10.01)	-35.99 (0.15)	-12.20 (1.04)	141.50 (0.07)
	8	30	0.28	34.50 (7.32)	-1.44 (1.62)	146.26 (10.46)	1.16 (7.66)	-11.53 (1.97)	194.26 (7.05)	-37.56 (0.18)	-13.11 (0.94)	140.88 (0.06)
				Mx (AP)	**My/ML**	**Mz/vert**	**Mx/AP**	**My/ML**	**Mz/vert**	**Mx/AP**	**My/ML**	**Mz/vert**
DUP	6.5	27	0.33	1.15 (0.28)	-3.22 (0.90)	-0.25 (0.06)	-0.03 (0.26)	-3.54 (0.82)	-0.25 (0.06)	-0.82 (0.11)	-0.19 (0.63)	-0.20 (0.05)
	7	29	0.32	0.81 (0.21)	-0.95 (1.18)	-0.13 (0.07)	-0.25 (0.22)	0.15 (0.83)	-0.02 (0.07)	-0.79 (0.16)	1.42 (0.67)	-0.08 (0.05)
RSP	6.5	32	0.33	1.24 (0.33)	-6.83 (1.26)	-0.38 (0.08)	-0.65 (0.37)	-1.34 (1.10)	-0.08 (0.06)	-0.69 (0.18)	3.90 (0.78)	0.19 (0.05)
	7	26	0.30	0.98 (0.37)	-5.69 (1.35)	-0.32 (0.09)	-0.57 (0.36)	0.08 (1.20)	-0.00 (0.07)	-0.89 (0.25)	5.11 (1.09)	0.24 (0.08)
	7.5	27	0.29	1.11 (0.48)	-6.13 (1.91)	-0.33 (0.10)	-0.19 (0.46)	-0.43 (1.28)	-0.02 (0.07)	-0.78 (0.15)	5.10 (1.04)	0.24 (0.07)
	8	30	0.28	1.23 (0.37)	-7.24 (1.53)	-0.36 (0.08)	-0.07 (0.36)	-1.56 (1.24)	-0.09 (0.07)	-0.95 (0.18)	4.87 (0.94)	0.20 (0.06)

Walking on DUP versus RSP

Figure 11 shows the temporal load distributions of walking trials on both DUP and RSP. Forces in the AP and ML directions are all similar between DUP and RSP for walking. Peak vertical force of the RSP is smaller compared to the DUP, vertical force on the RSP is more evenly distributed between peaks during absorption and propulsion. Temporal distribution of moment about the AP axis for DUP and RSP is similar, peak moments during both absorption and propulsion phases are slightly higher for RSP compared to DUP. Peak moment about the ML axis during both absorption and propulsion phases are higher for the RSP compared to the DUP during walking. Especially the peak moment during the initial absorption phase for the RSP is higher.

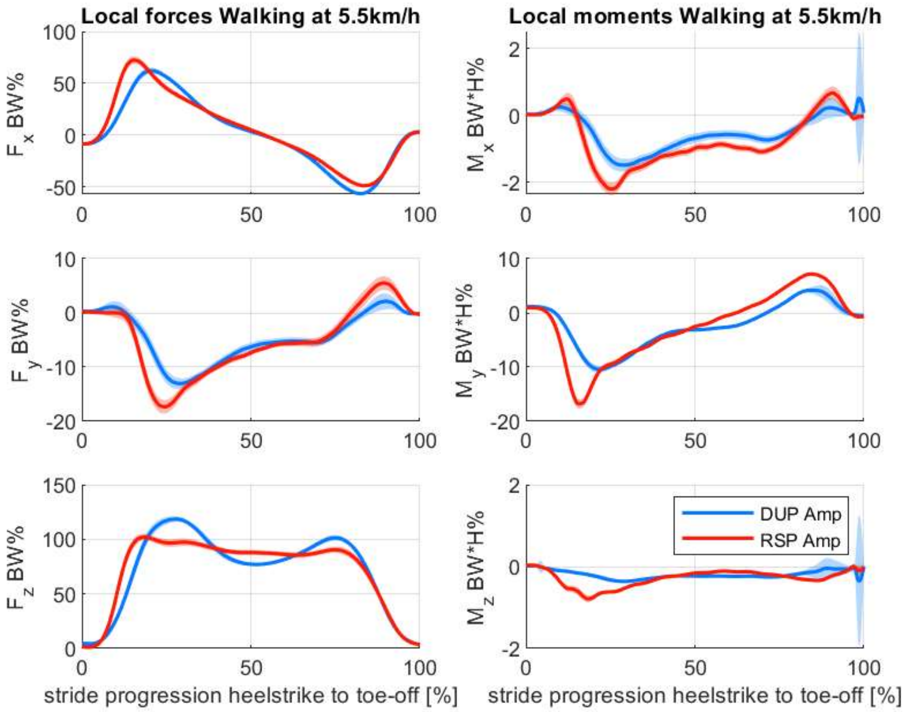

Figure 11: Mean local forces and moments during walking at 5.5km/h from HS to TO. Shaded area represents a single standard deviation determined from individual strides.

Running on RSP at variable speed

Figure 12 shows the temporal load distributions of running trials on the RSP for varying running speeds, the overall response of the loads to increasing running speed was small. Forces in AP and vertical direction increase minimally for increasing running speeds, mediolateral forces do not show a clear response to increased running speed. AP and ML moments during absorption phase increase minimally with increasing running speed. The peak AP and ML moments during propulsion phase do not increase at all when increasing running speed past 7.0km/h.

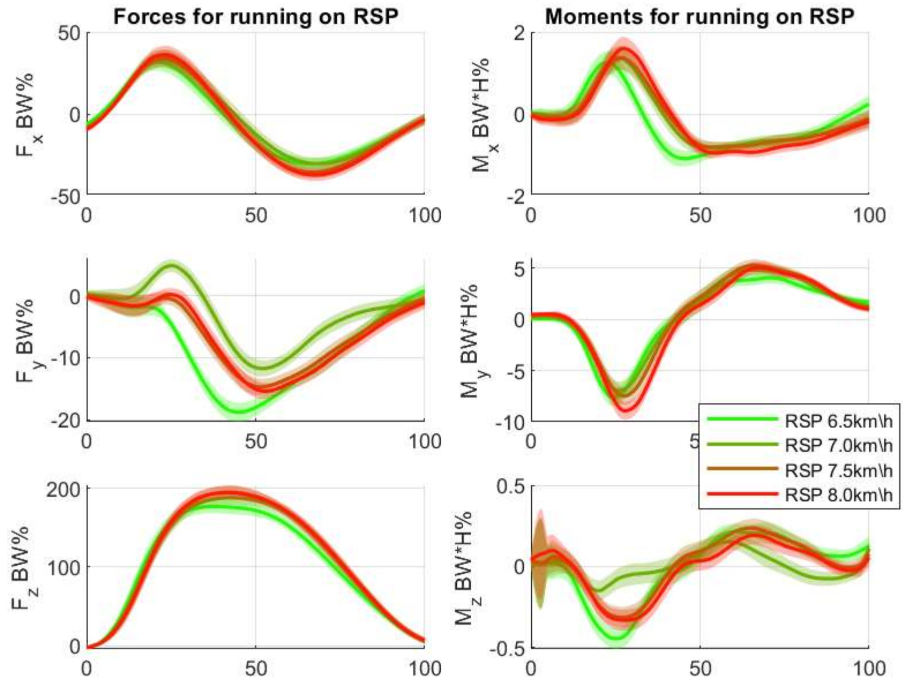

Figure 12: Average loads during stance phase of running at varying speed. Shaded area represents a single standard deviation determined from the individual strides.

Ground reaction forces

Figure 13 shows the ground reaction forces during stance phase with the effects of a DUP and RSP and the difference between amputated and intact leg for both a walking and running trial. Table 3 presents the peak GRFs during absorption, midstance and propulsion phases. For both walking and running the intact side shows good temporal resemblance for both the DUP and RSP and minimal differences in peak values.

The mediolateral GRFs for the amputated side of the RSP show equal values for peak medial forces during the absorption phase, but lower forces during propulsion. Braking and propulsion forces are higher for the RSP compared to the DUP for both walking and running. Braking forces of the RSP amputated side are equal to the intact leg in contrast with the DUP amputated side which is lower compared to the intact side. The propulsion force of the RSP amputated side is higher compared to the DUP, but also lower compared to the intact leg.

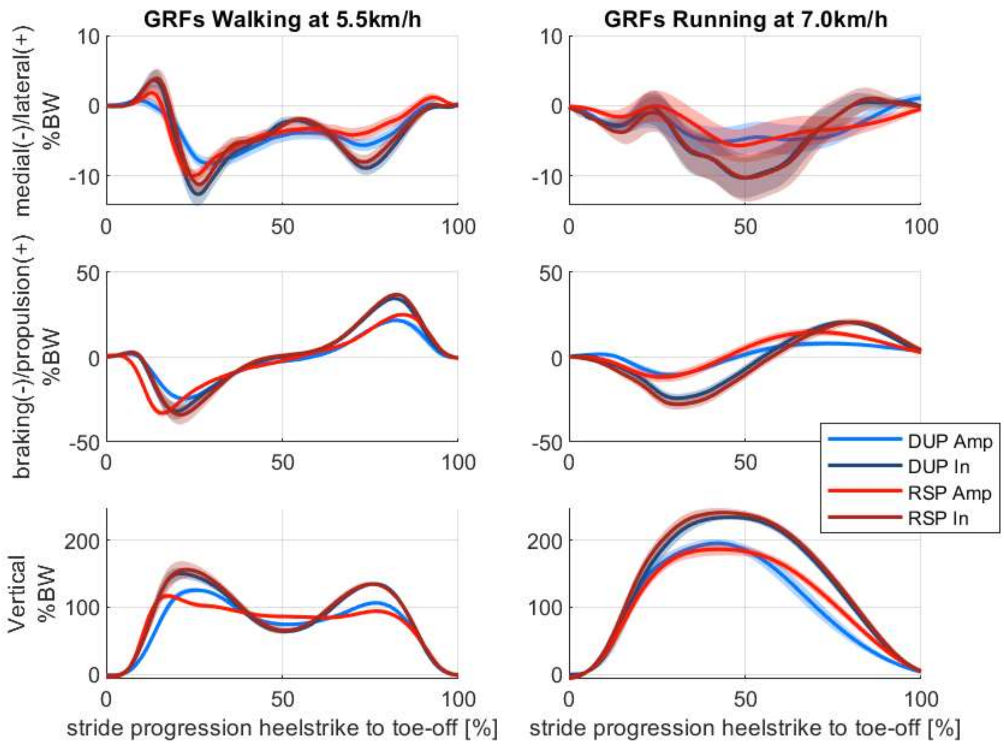

Figure 13: Ground reaction forces during stance phase for walking (left) and running (right) in percent body weight (BW). Daily Use Prosthesis (DUP) is represented in blue and Running Specific Prosthesis (RSP) in red. Both the ground reaction forces for the amputated leg (Amp: left) and intact leg (In: right) are shown. Mean forces are shown as a factor of body weight with a shaded area representing a single standard deviation over all valid strides in the trial.

The vertical GRFs in the amputated side are lower compared to the intact side for all conditions. The RSP shows lower peak vertical forces for walking during both absorption and propulsion phases, but higher force during midstance. A similar effect is present in the running trials, where the peak vertical GRF is lower for the RSP compared to DUP, but higher for the RSP during propulsion.

Increasing running speed has no clear effect on the mediolateral GRFs. Vertical GRF increases substantially over running speed for intact limb, but minimally for the prosthetic side (Figure 14). The increase in running speed from 6.5 to 7.0 km/h is reflected in an increase in anterior propulsion GRF for the amputated side, and limited increase in propulsion force for the intact side. The increase of speed from 7.0 to 7.5 and 8.0 km/h results in only a minor increase of propulsion GRF in the amputated leg, but substantial increase in the intact side.

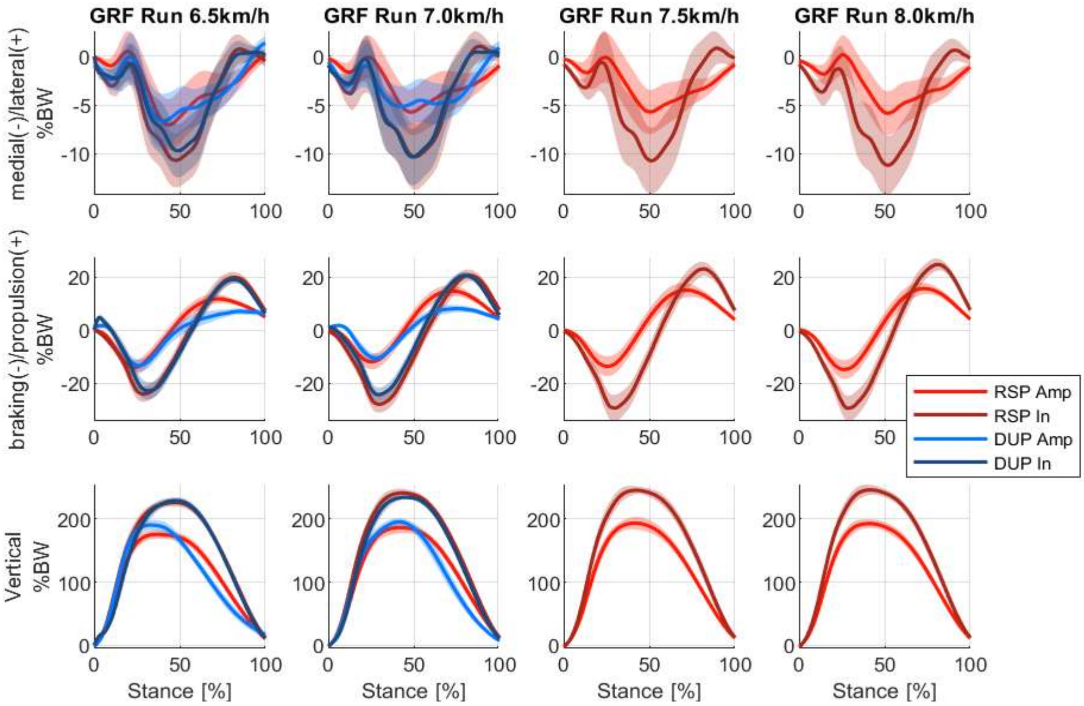

Figure 14 Ground reaction forces at varying running speeds and prostheses during stance phase in percent body weight (BW). red indicating the trials performed on the RSP, blue on the DUP. darker shade represents the intact leg and lighter shade the prosthesis.

Table 3 Mean and standard deviation (SD) of peak ground reaction forces during walking and running trials normalised to percentage of body weight. Amp and Int, indicates the amputated or intact side. Forces are expressed in a global reference frame. Greyed out area refer to the load cases used for the main comparison in Figure 10

					Absorption			**Midstance**			**Propulsion**		
	Speed	Prosthesis	Side	n	ML	AP	Vertical	ML	AP	Vertical	ML	AP	Vert
Walking	4.75	DUP	Amp	30	-5.45 (1.36)	-19.40 (1.56)	112.63 (3.96)				-3.73 (1.18)	18.74 (0.75)	97.81 (3.40)
			In	29	-5.68 (2.23)	-23.04 (5.04)	127.34 (12.58)				-5.15 (1.43)	27.84 (1.36)	109.19 (5.05)
	5.5	DUP	Amp	20	-4.70 (1.14)	-24.46 (1.38)	122.27 (4.79)				-3.61 (0.82)	21.74 (0.91)	95.17 (2.19)
			In	24	-5.58 (1.54)	-31.76 (5.02)	149.35 (9.40)				-5.71 (1.20)	34.65 (0.73)	120.35 (3.16)
		RSP	Amp	11	-0.03 (1.63)	-32.91 (1.79)	114.28 (4.80)				-1.43 (0.86)	25.06 (0.85)	78.61 (3.16)
			In	15	-5.84 (1.91)	-33.96 (5.70)	155.06 (13.61)				-4.36 (1.06)	36.93 (1.08)	113.73 (3.86)
running	6.5	DUP	Amp	27	-1.84 (2.54)	-13.25 (2.30)	184.67 (9.30)	-5.43 (2.64)	-10.94 (2.50)	190.44 (8.17)	-2.05 (1.01)	7.05 (1.22)	45.24 (7.28)
			Int	27	-5.47 (2.57)	-22.78 (3.30)	205.91 (10.42)	-9.62 (2.73)	-11.39 (2.52)	229.13 (5.22)	-0.18 (1.57)	19.05 (1.54)	105.37 (5.99)
		RSP	Amp	32	-2.44 (2.36)	-10.50 (1.68)	175.39 (9.39)	-5.12 (2.05)	-3.64 (1.55)	195.63 (5.79)	-4.47 (1.45)	8.08 (1.38)	83.65 (10.67)
			Int	32	-4.48 (2.87)	-24.21 (2.65)	209.51 (11.56)	-9.65 (2.90)	-13.04 (2.65)	234.24 (2.94)	-0.57 (1.85)	20.55 (1.28)	114.06 (6.14)
	7	DUP	Amp	29	-0.06 (2.18)	-13.97 (2.73)	156.63 (9.19)	-5.72 (2.55)	-6.99 (2.73)	175.68 (6.89)	-3.63 (1.93)	11.74 (1.68)	110.48 (7.08)
			Int	29	-5.79 (2.51)	-23.98 (2.94)	204.90 (8.98)	-10.66 (2.77)	-9.74 (2.94)	226.07 (6.14)	0.51 (1.68)	19.82 (2.04)	103.58 (7.16)
		RSP	Amp	26	-0.16 (2.22)	-11.85 (2.90)	159.50 (8.75)	-4.84 (2.22)	-2.27 (2.77)	186.50 (9.31)	-3.53 (2.02)	14.74 (2.06)	127.30 (7.12)
			Int	26	-4.45 (2.81)	-27.82 (3.14)	222.49 (10.32)	-8.62 (3.30)	-18.80 (3.06)	241.30 (6.65)	0.14 (2.09)	20.59 (2.18)	105.92 (8.01)
	7.5	RSP	Amp	27	-0.14 (2.57)	-13.61 (3.76)	165.41 (9.98)	-4.23 (2.54)	-3.59 (3.26)	193.48 (9.86)	-3.95 (1.63)	15.00 (2.67)	129.17 (7.28)
			Int	27	-4.07 (3.84)	-29.23 (4.92)	225.61 (13.01)	-8.42 (3.67)	-19.88 (3.98)	245.54 (6.35)	-0.54 (2.38)	22.97 (2.65)	115.63 (11.15)
	8	RSP	Amp	30	0.16 (1.99)	-14.77 (3.54)	169.50 (10.51)	-3.69 (2.21)	-5.83 (3.30)	192.76 (6.99)	-3.83 (1.67)	15.61 (2.15)	124.17 (7.02)
			Int	29	-3.38 (3.02)	-29.33 (4.69)	222.33 (11.65)	-8.45 (3.39)	-20.80 (4.29)	246.08 (8.20)	-1.08 (1.91)	24.63 (2.22)	117.93 (9.81)

4. Discussion

The primary aim of this study was to express the loads applied to the implant for running versus walking, DUP versus RSP and running at varying speed. Custom multibody models were used to process recordings of experimental trials to loads acting on a transtibial implant of a BAP. The results provide insight in the peak distribution of loads and acting on this implant during running.

Both forces in the transverse plane and bending moments are smaller during running compared to walking. Vertical forces are larger during running compared to walking. The effect of a DUP versus RSP during running had limited effect on the implant loads. AP forces for the DUP were more negative across the full stance phase. And ML moments were larger for the RSP compared to the DUP. Increasing running speed had a minimal effect on the implant loads and the GRFs of the amputated side. The GRFs on the intact side did increase with an increased running speed.

Based on the smaller bending moments during running, the risk of a bone fracture or device breakage during seems to be smaller for running compared to walking. However, vertical compression force is higher during running so the shear stress at the bone-implant interface might increase. It is not possible to say if the running of walking loads should be associated a higher risk of mechanical failure based on the combination of both findings.

It was expected that the implant loads would be more evenly distributed during running on the RSP compared to the DUP, this was not found. Instead, higher ML moments were found for the RSP compared to the DUP. This can be explained by a larger plantarflexion moment provided by the blade [40].

Increasing speed at lower running speeds (6.5, 7 km/h) affected the propulsive forces on the prosthetic side, but at higher speeds (7, 7.5, 8km/h) the main effect was an increase of propulsion forces in the intact limb. Somehow the running strategy of the participant resulted in offloading of the prosthetic. The exact cause is unknown, but it could be a cautious running technique where the participant is actively or subconsciously offloading the prosthetic limb. Since the participant didn't run for years, it could also be the case that the muscles of the hip and knee joints were not strong enough to provide more propulsive forces. Adaptation to regular running could in both cases alter the effects of varying running speed on the implant loads.

The reference frame for the implant loads is similar to a frame used by D'Angeli et al. [31] to determine local load along the tibia shaft in healthy subjects. In the present study, forces and moments are expressed at a single height located at the distal end of the DCA. The temporal load distribution of moments about ML and AP axes correspond well with the moments found by V. D'Angeli et al. [31].

The effects of intact versus amputated side and DUP versus RSP on GRFs in this study correspond with literature for the running condition [40]. Propulsion and absorption GRFs were reported to be higher for the intact limb versus DUP indicating compensation for the lack of force produced by the ankle. The different total GRF and especially the vertical GRF might indicate that the subject is modulating load distribution over both sides by compensating with the intact leg to reduce load in the prosthetic side. A better understanding of this strategy is important to understand the consistency of load on the prosthetic side. It was observed that the participant modulated running speed by increasing efforts in the intact limb and minimally in the prosthetic side. This effect resulted in substantially smaller forces on the prosthetic side. If this running strategy were to alter due to familiarisation with running and increased confidence, this could result in increased loads on the implant. This should be monitored carefully to allow timely intervention.

Asymmetry of gait between intact and amputated sides was affected by the type of prosthesis. Propulsion GRF was higher for RSP compared to DUP. This is reasonable, as the flexure of the blade stores energy in the blade like a spring, which is released during propulsion resulting in a higher prosthetic joint moment. It is also found [40] that improving propulsion in the prosthesis improves knee and hip work symmetry resulting in a better distribution of load over the joint.

The present study analysed the cyclic loading during gait on a level treadmill. Running outdoors on an uneven surface, accelerating, braking, and making turns during running are all expected to affect the implant loads. For translating the findings in our gait lab, it is required to assess these effects.

The sample size of one participant is small and the results of this study are patient specific, so it is not possible to draw conclusions on the effects of the varying conditions for other amputees. It should also be noted that the prosthetic alignment is tuned to the gait of the amputee by a CPO analysing kinematics. Minimising moments acting on the prosthesis is not the primary target in aligning the prosthesis [43]. Variance in gait and running technique also affects the load applied on joints [47]. Variance in implant loads during walking and running among amputees is therefore expected.

GRF and kinematic signals are subject to noise and a multibody model also induces errors and uncertainties. An alternative approach to this would be to use a force transducer to directly measure forces and moments in a local frame, such a system has already been developed and used in other studies [43,48,49] for SSPs and transfemoral BAPs. However, the transtibial BAP has very limited build height which does not allow the installation of such a transducer. A force transducer of smaller form factor could be a solution for the build height and provide improved measurement accuracy.

This study is the first to present loads acting on the implant obtained from experimental data. This data can be used for further analysis with the aim to provide a subject specific advice if it is safe to run on a BAP for our participant.

Two custom multibody models were created for the different prostheses to determine the loads in a uniform reference frame located near the implant. The main findings of this analysis were that the bending moments acting on the implant were larger during walking gait compared to running gait, but the axial compressive forces were larger during running. Temporal load distribution was different between DUP and RSP, but magnitudes were similar. The effect of increased running speed resulted in an increased ground reaction force for the intact limb, but the effect on the prosthesis side was minimal.

The exact response of the loads transmitted from implant to the bone remains complex and difficult to analyse since the exact interface forces are not directly measurable. A FEM model for the in-vivo system of the implant and bone of the participant could improve insight in the loads on the bone-implant interface and distribution of load along the tibia.

Section 2: Finite Element Analysis of Load Distribution in a Tibial Bone-Anchored Prosthesis During Running

Keywords: bone anchored prosthesis; finite element analysis; Osseo integrated implant; running; amputation patient; implant loading

Abstract

Clinical practice has proven that a bone anchored prosthesis is a viable alternative to a socket suspended prosthesis for transtibial amputees experiencing chronic skin problems. However, limited knowledge is available of the mechanical limits of the bone implant system. This study aimed at investigating the load distribution and risk of bone failure of a transtibial bone anchored prosthesis under running loads using finite element analysis. An earlier study by our group investigated obtained loads of running on a bone anchored prosthesis based on experimental measurements and multi-body dynamic analysis, which was used as preliminary work. Mechanical properties of bone were extracted from CT data and used to develop a subject specific finite element model of the bone implant system. The distribution pattern of stress and stress/strength ratio were simulated and compared between walking and running. Similar distributions were found for the phases of gait. The peak and overall magnitude of stress and stress/strength ratio were substantially larger for the walking load case compared to the running load case. No substantial differences in stress were observed between running on a conventional prosthesis foot and a blade. Our results indicate that there is no increased risk of bone fracture during running compared to walking using a tibial bone-anchored prosthesis.

1. Introduction

A bone-anchored prosthesis (BAP) consists of an artificial limb that is connected to an implant which is integrated in the intramedullary cavity of a bone. It relies on osseointegration for anchorage of the implant in the host bone[50]. The fixation is achieved by bone ingrowth on the surface of the implant which is designed with a porous surface to promote contact area between implant and bone tissue[51].

Mechanical failure modes for BAPs in general are identified as periprosthetic fracture, septic and aseptic loosening or device breakage [33]. These have been reported mainly for transfemoral BAPs[27]. Survival rates of transtibial BAPs are mentioned, but underreported, in literature and cause of failure is often missing [27]. Of the reported explantations for transtibial BAPs, causes are attributed to septic loosening [52]. Experiences with TT BAP regarding mechanical failures are positive despite the lack of reported outcomes in literature. Reported periprosthetic fractures in femoral implants are attributed to excessive loads occurring during a fall [27].

Large interest in the limits of permitted activities exists among amputees, with special interest in running. However, much is unknown about the load transfer at the bone-implant interface. It is assumed that the loads on the bone-implant system are higher during running compared to walking due to the dynamic nature of the running activity. Hence, the prescriptions of allowed activities are very conservative, i.e. excluding running, due to the high risks associated with mechanical failure of the system. However, loads acting on the bone-implant system during running have never been explicitly investigated.

Looking at the literature, in a case study, loads acting on an implant-adapter system have been experimentally determined in a gait lab [53]. Comparing load magnitude during running to walking provided the insight that bending moments were smaller during running, however axial forces on the system were higher in running compared to walking. Implications of these findings on the distribution of stress in the bone and at the bone implant interface have not been studied.

Galteri et al. presented a comprehensive overview of recent efforts made to characterise the bone-implant system for femurs using a variety of ex vivo and in silico models [33]. Much effort was made to study osseointegrated systems in these femurs using finite element (FE) models where stress distribution in the bone was the main outcome. The osseointegrated implants for transtibial amputations have not been studied using FE models as much as was done for femur implants. Validating a model for the in vivo bone implant interface remains a challenge limiting interpretations of the simulations due to lack of validation. Therefore, assumptions on the bone implant surface have to be made when describing the osseointegrated system using a FE model.

The aim of this study is to construct a FE model of the tibial implant bone system and apply load cases consisting of peak forces and moments during walking and running. Outcomes of these simulations are spatial stress distribution, peak stress and the margin of simulated stress to the local yield stress. Comparing these outcomes between walking and running where walking serves as a baseline may provide more insight in the risks associated with running on a transtibial BAP.

2. Materials & Methods

A single subject performed walking and running trials at different speeds. Details about these experiments are described in a previous study by our group [53]. Forces and moments were determined at peak axial forces during absorption and propulsion phases for walking. For running, loads were determined at the peak axial force located at midstance during running and at peak bending moments in both absorption and propulsion phases. These loads were used in the FE simulations.

Modelling workflow

The FE model was created in MSC Marc Mentat 2023.2 from a tibia mesh obtained from CT and implant obtained from a computer aided design (CAD) model. Simulations were performed under the assumption of linear elastic material properties which was evaluated post-simulation by comparing von Mises stress to yield stress. The diagram in Figure 15 illustrates an overview of the individual steps taken to obtain the model.

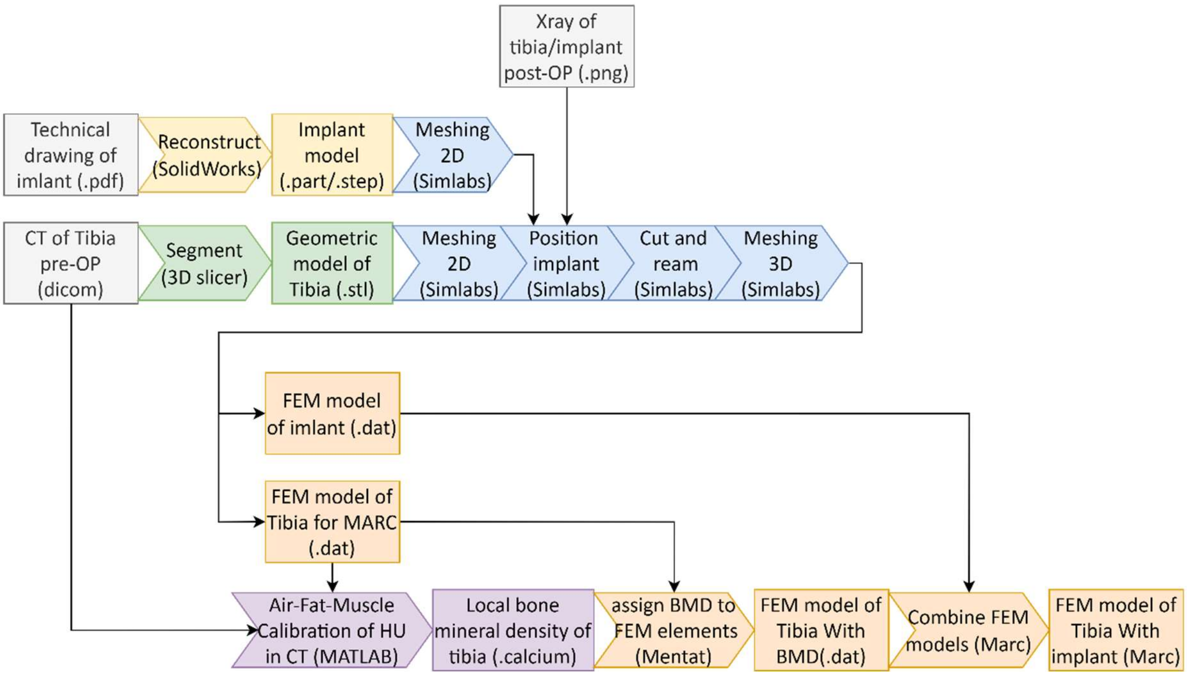

Figure 15: Workflow of constructing the FE model. Squares represent a file with the format indicated in brackets, arrow boxes indicate a process where the associated software is indicated in brackets.

2.1 Components and geometry

Implant geometry and properties

The participant in this case study received a personalised BADAL X® OTI intramedullary implant (OTN implants B.V.) more than 3 years prior to the experiment and was comfortable with walking on a prosthesis. The implant was produced using selective laser melting (SLM) of a grade 5 titanium alloy (TI6Al4V). The design of the implant was tested conform ISO 10328 standards in which the implant was loaded 10 million times with 175kg at 4Hz where the load application is at the maximum allowed offset. The implant consists of a solid titanium core with a diameter of 16.0mm with a porous surface consisting of a lattice structure. The CAD model of the implant was adjusted to exclude the lattice surface, the holes for transverse screws and the distal taper receiver filled to obtain a simplified solid model.

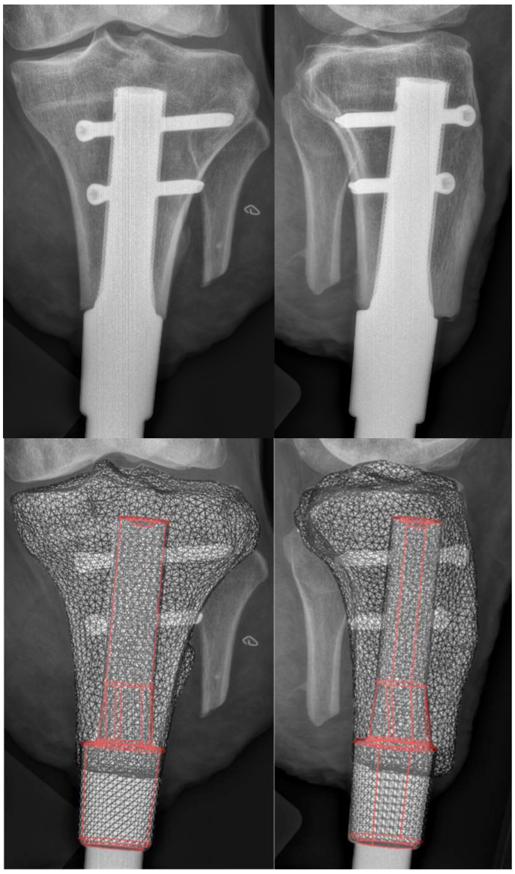

Figure 16: Illustration of implant positioning in postoperative Xray. Top figures are X-rays of frontal and lateral view. In bottom figures the segmented tibia and implants are overlaid. Note that the distal end of the tibia is not yet shortened.

Bone implant model

A 3D surface bone model of the tibia was obtained by segmenting a CT scan using 3D slicer software [54]. The CT scan with slice thickness 0.5mm was obtained three months pre-operatively. The steps of combining the tibia and implant were analogous to the implantation surgery and were performed virtually in the software ALTAIR SIMLABS 2023.1. The implant was positioned and aligned in the tibia to match post-operative X-ray images. The distal end of the tibia was cut transversally to match the length in the post-operative X-rays. A duplicate of the implant model was used in a Boolean operation on the tibia to remove the intramedullary cavity of the tibia model.

2.2 Meshing

The software Altair SIMLABS (Altair Engineering Inc.) was used to generate separate surface meshes for both tibia and implant consisting of first order triangular elements. A FE mesh of first order tetrahedral elements was then generated with an average edge length of 2.5mm, in analogy to the material model of Keyak et al. [55] for both tibia and implant model, resulting in 75372 and 10647 elements for the respective models.

2.3 Material laws and properties

For the tibia, mechanical properties were determined individually for each element based on the grey value intensity of the voxels in the CT-scan. These calculations were performed using MATLAB 2020a and a Fortan subroutine in conjunction with Marc (MSC software). To convert Hounsfield Unit (HU) to bone mineral density (BMD), the methodology and reference values from Eggermont et al. [56] were used. The HU intensity peaks of air, fat and muscle tissue in the CT are determined for a region in the

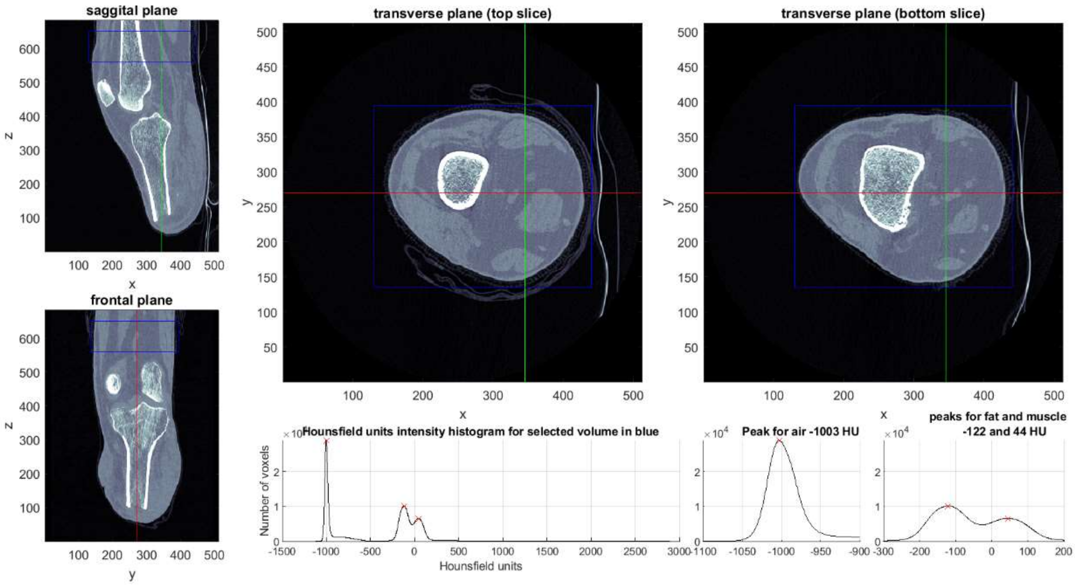

Figure 17: Anatomical cross sections of the CT scan with a local selection highlighted in blue from which the air fat and muscle tissue HU values are used for the transformation of HU to BMD. Green: coronal plane, red: sagittal plane, blue: selected volume of healthy tissues.

upper leg containing healthy tissues (Figure 17). The following transformation of HU to BMD was found within the standard deviation reported by Eggermont et al. [56]:

$$BMD = 1.1872 * HU - 8.1248$$

Each element of the tibia model is matched to corresponding voxels in the CT to determine average BMD of the element (Figure 18). Relations to assign mechanical properties are found by Keyak et al. [55], $E = 14900\rho_{ash}^{1.86}$, $S = 102\rho_{as}^{1.80}$. To apply these relations, a transformation from BMD to ash density is required, $\rho_{ash} = 0.0633 + 0.887\rho_{BMD}$ [55].

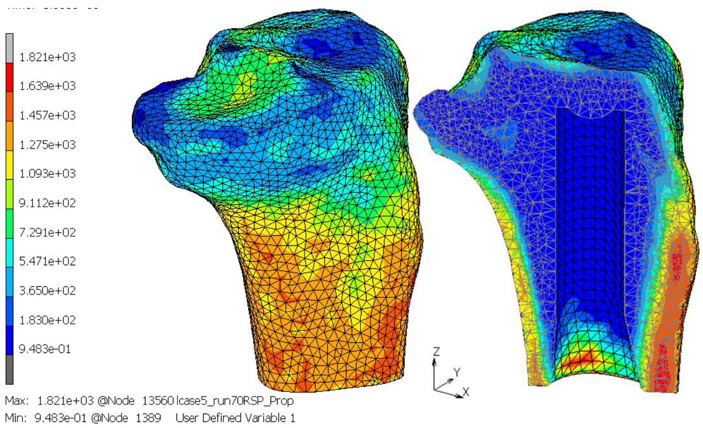

Figure 18: FE model of tibia without Implant with heatmap of BMD.

Material properties of the implant were obtained from a datasheet[57] of SLM manufactured Ti6Al4V (grade 23) which is also corresponds well with values found in literature[58]. The material is assumed isotropic with a Young's modulus of 115GPa and Poisson's ratio of 0.34. It is assumed that after 3 years using the BAP in daily life, osseointegration resulted in a rigid fixation of implant in the tibia. Implant and tibia models are bonded node-to-node resulting in direct load transfer without contact interaction. Hence, the implant model was bonded along the shaft of the implant, but not at the distal osteotomy face as a minimal gap between these interfaces was visible in the x-rays.

2.5 Boundary conditions

Proximal fixation of the model on the surface nodes results in artefacts at the boundary of the fixation. To prevent this effect from occurring near the region of interest, the proximal end of the tibia should be fixed at least one diameter length from the proximal tip of the implant. In the model of this study, this was not possible due to the limited length of the tibia and length of the implant (Figure 19). Therefore, the tibia is proximally fixated by constraining the surface nodes of the proximal face of the tibia. This corresponded to all surface nodes above 5mm of the proximal tip of the implant. This method will result in stress concentration at the boundary of the selected surface.

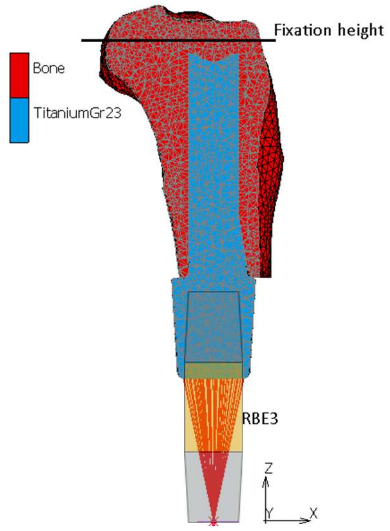

Figure 19: Sagittal cross section of the FE model. Tibia is coloured red, implant blue. Transparant overlay of the dual cone adapter for reference and not included in the FE model.

Peak loads (Table 4) were determined for walking and running with DUB and RSP by our group [53]. These loads were applied to a reference node located in the extension of the implant at the position of the distal end of the dual cone adapter where the load is defined [53]. The load is distributed over the distal end of the implant using a (rigid body equivalent) RBE3 link.

Table 4: Load cases of walking and running on daily use prosthesis (DUP) and running on a running specific prosthesis (RSP). Loads are specified for each gait event, Abs: peak force during Absorption, Mid: peak force during Midstance, Prop: peak force during propulsion

Mode	Prosthesis	Speed [km/h]	Phase	Fx [N]	Fy [N]	Fz [N]	Mx [Nm]	My [Nm]	Mz [Nm]
Walking	DUP	5.5	Abs	325.36	-84.92	778.81	-16.31	-100.60	-3.94
			Prop	-287.23	-26.23	665.59	-7.16	14.47	-2.70
Running	DUP	7.0	Abs	55.57	-44.69	1137.59	12.05	-49.91	-2.64
			Mid	-160.54	-104.85	1290.94	-2.76	1.70	-0.23
			Prop	-294.17	-105.92	1040.16	-8.74	15.72	-0.83
Running	RSP	7.0	Abs	180.84	-24.70	1040.61	12.45	-74.81	-3.98
			Mid	-25.86	-94.08	1235.26	-6.34	0.91	-0.04
			Prop	-241.12	-88.28	953.36	-9.98	56.40	2.72

2.6 Statistical analysis

The aim of this study is to assess the risk of local bone failure under different conditions. This is evaluated by assessing the stress distribution and risk of local bone failure. Due to the complex multiaxial stress in these load cases, the Von Mises stress criterion is used to assesses the stress distribution. Yield strength characterises the threshold for the transition from elastic to plastic deformation. To determine the risk of bone failure, the yield criterion of the local bone tissue is used. The Von Mises yield criterion is used as it combines multiaxial stresses into a single value that can be assessed using the local strength.

Plastic deformation in bone tissue would result in plasticity of the tissue. Bone is capable of sustaining plastic deformation to a certain degree but will fracture after a certain amount of plastic load cycles. In cyclic movements like walking and running, this damage would accumulate too fast and pose a serious risk of fracture, stress should therefore not surpass the yielding criterion[59]. This condition is reflected in assessing $\frac{\sigma_{vm}}{S} < 1$. Where σ_{vm} indicates the Von Mises stress [Pa] and S indicates the strength [Pa]. It should be noted that during elastic deformations, microdamage can also accumulate but at a much lower rate. A safety factor is normally considered for assessing stress strength ratios in structural engineering, however as walking on the DUP is considered as a baseline, no safety factor is incorporated. It is also hypothesised that under the assumption of sufficient recovery, microdamage induced by elastic deformations is repaired by bone remodelling without accumulation[60]. Both the von Mises stress and the strength are approximations for which assumption are made. The computed values can therefore not be trusted directly, however by comparing these values to a clinically successful case, an assessment of the change in risk of failure can be made.

3. Results

Simulations were performed for all load cases shown in Table 4. The spatial distributions of von Mises stress and stress/strength ratio in the tibia are presented in Figure 20 and Figure 21 respectively. The peak von Mises stress and stress/strength ratio are presented in Table 5 and Table 6, respectively.

Von Mises stress

Simulations resulted in concentration of von Mises stress along the cortex and on the bone-implant interface (Figure 20) for all load cases (Table 4). Stress also concentrated at the edge of the proximal fixation boundary condition. Stress distribution differed between absorption, midstance and propulsion load cases by concentrating stress at the anterior or posterior sides of the cortex and implant interface. Peak stress values were found at the distal posterior interface (Figure 20) or at the anterior surface at the edge of the proximal fixation boundary condition. Peak von Mises stress values for all simulated load cases are given in Table 5. The Von Mises stress representation in transverse cross sections for the absorption, midstance and propulsion for the different load cases are given in Appendix A.

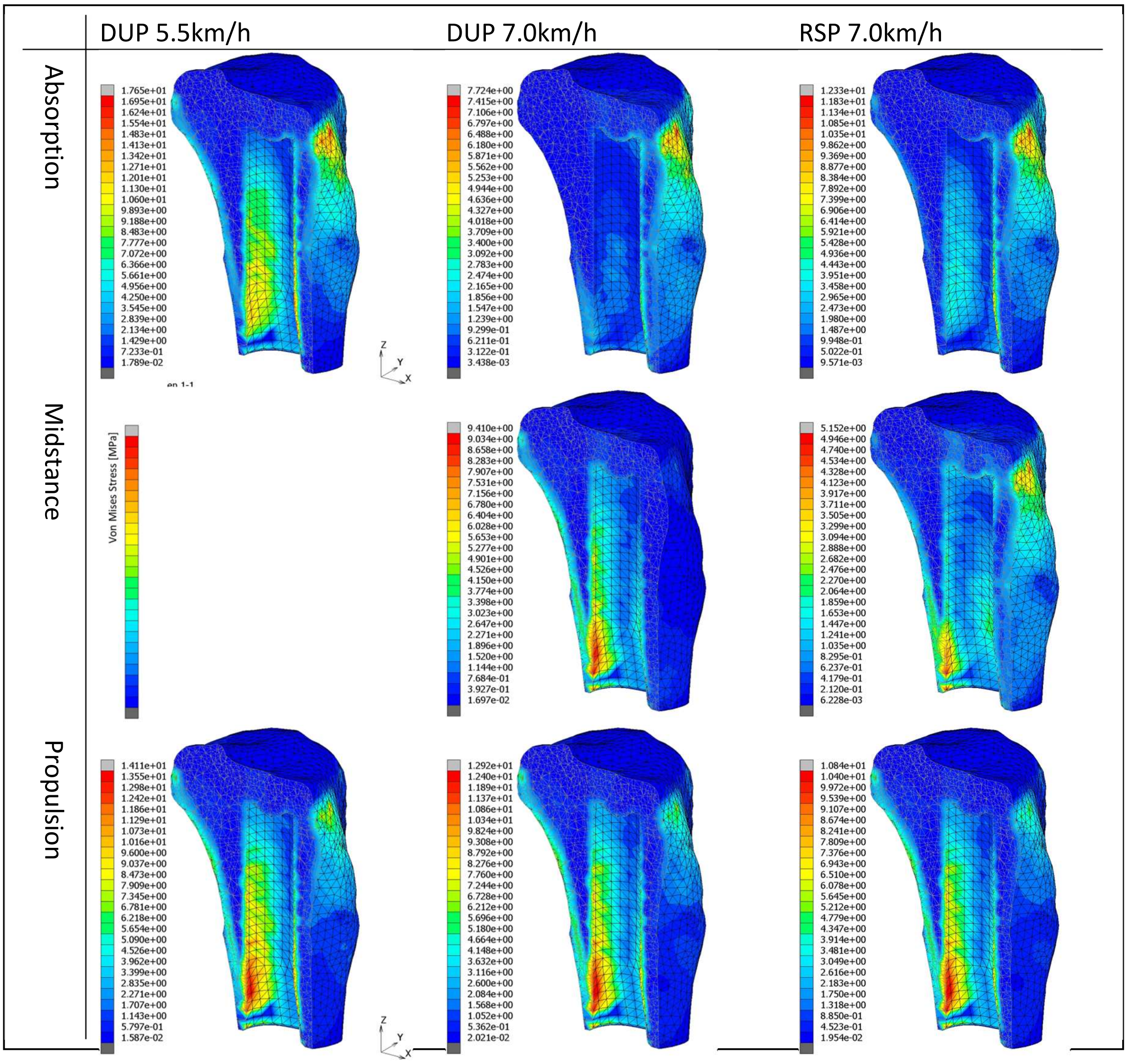

Figure 20: Von Mises stress [MPa] visualised in a sagittal cross section. Scales are not uniform to illustrate the distribution for each load case separately.

Peak von Mises stress	DUP walk [MPa]	DUP run [MPa]	RSP run [MPa]
Absorption	18.03	6.21	9.69
Midstance	-	12.40	7.83
Propulsion	14.21	15.66	13.06

Table 5: Peak von Mises stress in the tibia for different load cases reported in [MPa]

Stress/strength ratio

As shown in Figure 21, the stress/strength ratio is increased in the trabecular bone of the proximal tibia. Peak values for the stress/strength ratio were located at the proximal tip of the tibia for all load cases. For absorption load cases where a negative bending moment was applied on the system, the peak stress/strength ratio was located anteriorly. For propulsion load cases with a positive bending moment the peak ratio was located at the posterior proximal tip of the implant. For the midstance load case of the DUP running condition, the stress/strength ratio was distributed similar to the propulsion load case but of lesser magnitude. The peak stress/strength ratio for the midstance load case for running on RSP was evenly distributed at the proximal end of the tip of the implant.

All simulated stress/strength ratios were smaller than 0.5 (Table 6) indicating a minimum safety factor of 2. Peak values of stress/strength ratio during absorption are larger for the walking load case compared to both running load cases. Difference in ratio between the DUP and RSP was small.

The highest stress/strength ratio values were found during absorption in the case of DUP walking. For running in the DUP highest stress strength ratio was found during propulsion, and for running on the RSP during absorption (Table 6). Distribution of the stress/strength ratio across the full tibia is represented in Figure 22 with transverse cross-sections for the highest. The transverse cross-sections for all load cases are given in Appendix B.

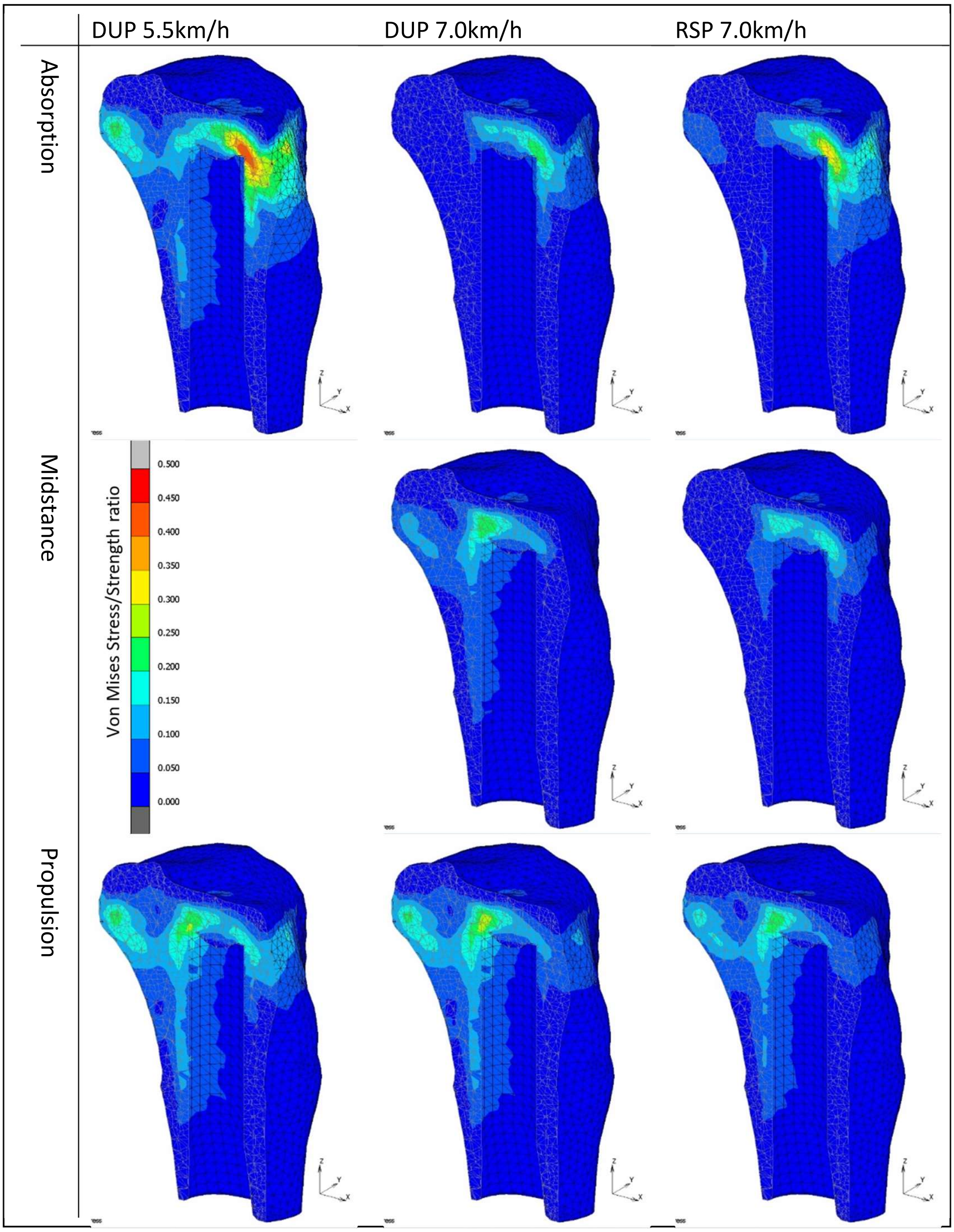

Figure 21: Stress/strength ratio visualised in a sagittal cross section for all load cases. Uniform colour scale ranging from 0 to 0.5 is used for all models.

Table 6: Peak stress/strength ratio [-] in the tibia for Daily use prosthesis (DUP) walking and running and running specific prosthesis (RSP)

Peak stress/strength Ratio	DUP walk	DUP run	RSP run
Absorption	0.468	0.249	0.335
Midstance	-	0.266	0.223
Propulsion	0.274	0.284	0.245

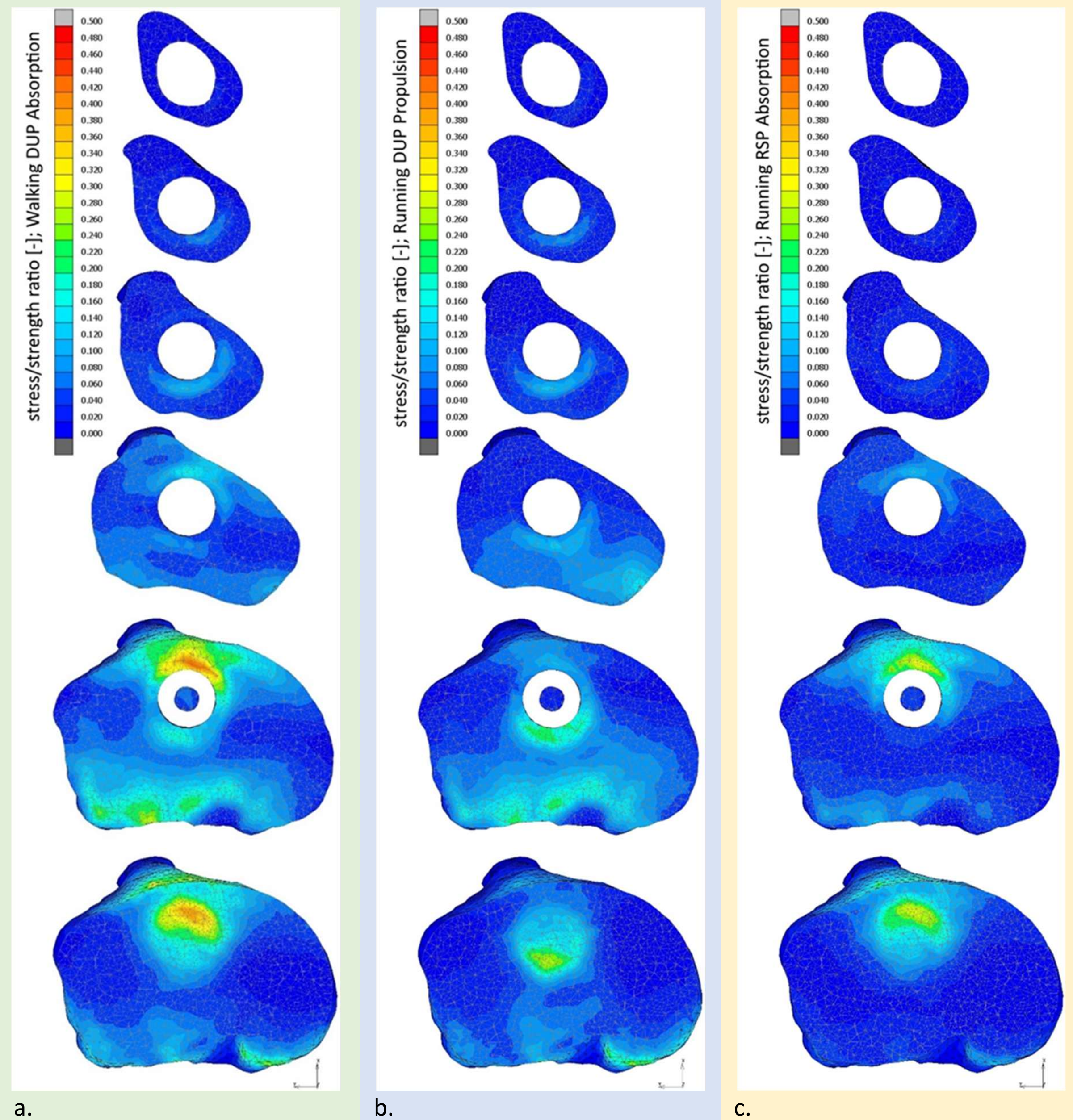

Figure 22: Von Mises stress/strength ratio for phases in which the highest stress/strength ratios were found (Table 6), presented in transverse cross sections of the tibia at +10, +25, +40, +55, +70, +75mm offset from the distal tip. Uniform colour scale ranging from 0 to 0.5 is used for all figures presenting the stress/strength ratio. (a.) shows the stress/strength ratio for load case walking with Daily use prosthesis (DUP) during the absorption phase. (b.) shows the stress/strength ratio for load case running with DUP during the propulsion phase. (c.) shows the stress/strength ratio for load case running with Running specific prosthesis (RSP) during the absorption phase.

4. Discussion

The aim of this study was to gain more insight in the risks associated with running on a transtibial BAP. This was done by analysing the spatial stress distribution, peak stress and stress/strength ratios in the tibia which followed from FE simulations of load cases from running and walking with a transtibial BAP.

For this case study, peak stress/strength ratio values in bone were not increased during running on a bone anchored prosthesis compared to walking gait. The load cases found in our previous study [53] (Table 4) showed that the bending moments applied on the implant were smaller during running, but the axial forces larger compared to walking. Results of FE simulations show a reduced stress and stress/strength ratio int the tibia for running compared to walking. Hence, the results of this study imply that the risk of bone fracture is not increased for this case when running on a transtibial bone anchored prosthesis.

Bone remodelling is the ongoing process of bone resorption and formation of new bone matrix. This process is moderated by the application of load, and damage to bone tissue [61]. It is a critical factor in the long-term success of BAPs. Previous research on transfemoral bone anchored prostheses has shown a positive response to loading the implant on the periprosthetic cortical thickness [62] and periprosthetic bone ingrowth [63]. However, the implant for a transtibial BAP is biomechanically different. The transfemoral implant is embedded in cortical bone in the diaphysis, but the transtibial implant is mostly enveloped by trabecular bone in the metaphysis with the tip already in contact with the epiphysis. The tibial implant transfers load from the prosthetic limb directly to the trabecular bone. Respecting Wolff's law, it is expected that the three years post operative the periprosthetic trabecular bone has adapted to the new loading situation by rearranging the orientation of trabeculae and adapting the mineralisation [64]. It is believed that this adaptation converges to an equilibrium in the remodelling process where a uniform stress distribution is achieved for the applied loads [65]. This effect is not included in the current study, but it is hypothesized that this process strengthens the bone resulting in even more even distribution of stress and more favourable stress/strength ratios which would reduce the risk on bone fracture further. However, no publications on bone remodelling of a transtibial BAP were found.

The present study assessed the condition of exceeding the yielding criterion for the bone under loads representative for running. This provides an assessment of the risk of direct fracture or fatigue failure of the bone. However, due to the cyclic nature of running there is also a potential risk of aseptic loosening which can only be evaluated partially from this study. Not one true cause of aseptic loosening is known in literature, but multiple theories have been proposed [66]. Theories include accumulation of microdamage at the interface as a result of repeated mechanical stress [67,68], inflammatory response to wear particles [66] and bone resorption as a result of stress shielding [69]. Results of this study indicated concentration of stress at the bone-implant interface, but deformations remained elastic below 0.5 stress strength ratio, so excessive accumulation of microdamage is unlikely. However, the true mechanical interaction of this interface is not valid due to simplifications. The simplified representation of the interface also does not allow predictions of wear. The distal end of the tibia is not deprived of stress, as the implant is bonded along the full length of the tibia. However, the stress/strength ratio at the distal end of the tibia is small, indicating offloading of the bone at the distal end. This could lead to bone resorption, and aseptic loosening in the long term. The distal tibia face was not modelled in contact with the tibia, load was only transferred at the implant shaft and proximal implant face. The post operative x-rays showed a slight gap between the tibia and implant collar. However, this gap might have altered post-operatively resulting in load transfer of the implant collar to the cortical bone at the osteotomy. A study of BMD adaptation after rehabilitation would provide insight into the possibility of this effect occurring.

The transverse screws that provide primary stability of the implant are not included in the model. These do however affect the load distribution which would affect the results found in this study. It is hypothesised that these screws distribute load from the implant to the cortical bone where the screws penetrate the cortex. Increased load transfer from the implant to the cortical bone could also result in less load transfer at the bone implant interface compared to the current model, resulting in less stress in the periprosthetic trabecular bone. Due to the substantially higher strength of the cortical bone the stress/strength ratio in the cortex would probably still not exceed values found in the trabecular bone.

The method of proximal fixation in the model is not ideal as the implant is located close to the tibial plateau. This affects the distribution of loads and concentrates stress at the edge of the fixation height. A more anatomical boundary condition could better represent the load distribution. This would require contact modelling of the femur and modelling of the insertions of tendons on the residual tibia, which is difficult to model and validate.

The presented model has several limitations that can constrain implications. Also, the context of experiments and validity of the model used in this study should be considered in the interpretation of the results.

The FE model is based on a CT scan three months pre-operative, this introduces discrepancies between the model and the experimental situation three years post-implantation. Positioning of the implant was performed manually using two Xray images of coronal and sagittal perspectives. Despite the best efforts to perform this positioning, it is prone to human error. Implants are also known to migrate post-implantation [20]. Both effects could reduce the validity of the model, if the implant was angulated differently in the model with respect to in-situ during the experiments, the forces and moments are transmitted to the tibia differently. The magnitude of this effect is unknown but expected to be limited. A segmentation of CT with implant in situ [63] would be a better method of defining the position and orientation of the implant in the model. This data was not available and would also pose challenges for the assignment of material properties of the bone due to metal artefacts.

Developing a novel method of constructing an in-situ based FE model, could resolve These discrepancies. If the metal artefacts can be resolved, a model of bone with implant in-situ could be able to better capture the mechanical properties of the bone after remodelling. No such method was found in literature; however, this might be possible by normalising the attenuation of metal artifacts using a pre- and post-operative CT. This method would also resolve the issue of manually positioning the implant.

The interface interactions between bone and implant are simplified as bonded under the assumption of perfect osseointegration. It is unknown whether full ingrowth in the bone on the implant interface is achieved but given the completed revalidation period and three years of use of the transtibial BAP by the participant of this study, it is assumed more likely to have full bone ingrowth as opposed to partial ingrowth the chances of high are estimated to be high. If this would not be the case, load transfer of bone of implant to the bone would occur over a smaller surface area resulting in higher local stress and in term also stress/strength ratio.

This study supports the hypothesis that it could be safe to run on a BAP. The applied modelling methods are in line with the state of the art [33]. All limitations considered, it is still believed that the results of this study, can lead to cautious steps towards higher demanding activities in rehabilitation for BAP users.

A Finite element model was created of the implant and the tibia. Loads from the gait analysis were applied to simulate stress distribution and spatial fracture risk. Local stress and stress-strength ratios were not larger for running compared to the walking load case. Local stress and stress-strength ratio distribution and magnitude were similar between the DUP and RSP.

The next proposed step is to evaluate the response to periodical running sessions in a rehabilitation setting. Perceived pain or other sensations should be monitored closely to mitigate any risks. Monitoring the tibia using X-rays would provide information on the response of the bone to the implant loading.

Conclusion

The presented study investigated the loads acting on a bone anchored prosthesis of a transtibial amputee in walking and running conditions aimed at assessing for risk of mechanical failure. Measurements were recorded on a daily prosthesis and a blade in a gait lab using motion capture and ground reaction force measurements.

Two custom multibody models were created for the different prostheses to determine the loads in a uniform reference frame located near the implant. The main findings of this analysis were that the bending moments acting on the implant were larger during walking gait compared to running gait, but the axial compressive forces were larger during running. Temporal load distribution was different between DUP and RSP, but magnitudes were similar. The effect of increased running speed resulted in an increased ground reaction force for the intact limb, but the effect on the prosthesis side was minimal.

A Finite element model was created of the implant and the tibia. Loads from the gait analysis were applied to simulate stress distribution and spatial fracture risk. Local stress and stress-strength ratios were not larger for running compared to the walking load case. Local stress and stress-strength ratio distribution and magnitude were similar between the DUP and RSP.

The findings of this study support the hypothesis that running on a bone anchored prosthesis can be safe for a transtibial amputee and do not advise against allowing the patient to run in a controlled setting. Due to the limitations of this study, it is advised to start small and keep evaluating the response of the patient to running in a rehabilitation setting. This provides beginning of the answer to the question if it is safe for the patient in our study to run again. Broad clinical implications of this study not possible, but a beginning can be made in experimenting if running is safe for transtibial BAP users.

Further addressing the identified limitations of the FE model is advised to improve model validity to get a better understanding of the biomechanics of the transtibial BAP.

The knowledge of periprosthetic bone remodelling for a transtibial BAP is limited. Most studies [21,34] reporting on periprosthetic bone remodelling investigated transfemoral BAPs. This allows for limited translation to transtibial BAP due to the different types of bone the implant is in contact with. More imaging data on the bone remodelling of the tibia in response to rehabilitation and walking loads on a BAP would already provide a better understanding of the response to habitual loading.

A next step after this study would be to improve the used modelling pipeline and include additional participants in a similar experiment. It was observed that the participant modulated running speed by increasing efforts in the intact limb and minimally in the prosthetic side which resulted in substantially smaller loads on the prosthetic side. If this running strategy were to alter due to familiarisation with running and increased confidence, this could result in increased loads on the implant. This should be monitored carefully to allow timely intervention. Assessing multiple participants allows analysis of different walking and running strategies in combination with different prostheses and alignments, also Different implant models could be investigated. One step further, these participants could be enrolled in a training regime of running in a controlled environment to analyse the response to repeated exposure of running loads. The bone remodelling response can be assessed using X-rays.

References

[1] Sinha R, Van Den Heuvel WJA, Arokiasamy P. Factors affecting quality of life in lower limb amputees. Prosthet Orthot Int. 2011;35(1):90–6.

[2] Moxey PW, Gogalniceanu P, Hinchliffe RJ, Loftus IM, Jones KJ, Thompson MM, et al. Lower extremity amputations - a review of global variability in incidence. Diabet Med. 2011;28(10):1144–53.

[3] McDonald CL, Westcott-Mccoy S, Weaver MR, Haagsma J, Kartin D. Global prevalence of traumatic non-fatal limb amputation. Prosthet Orthot Int. 2021;45(2):105–14.

[4] Frölke JPM, Rommers GMC, de Boer AW, Groenveld TD, Leijendekkers R. Epidemiology of Limb Amputations and Prosthetic Use During COVID-19 Pandemic in the Netherlands. Arch Phys Med Rehabil. 2024;105(2):280–6.

[5] CBS. Bevolkingsteller [Internet]. [cited 2024 Jun 21]. Available from: https://www.cbs.nl/nl-nl/visualisaties/dashboard-bevolking/bevolkingsteller

[6] Fortington L V., Rommers GM, Postema K, Van Netten JJ, Geertzen JHB, Dijkstra PU. Lower limb amputation in Northern Netherlands: Unchanged incidence from 1991-1992 to 2003-2004. Prosthet Orthot Int. 2013;37(4):305–10.

[7] Fard B, Dijkstra PU, Stewart RE, Geertzen JHB. Incidence rates of dysvascular lower extremity amputation changes in Northern Netherlands: A comparison of three cohorts of 1991-1992, 2003-2004 and 2012-2013. PLoS One. 2018;13(9):2003–4.

[8] Meulenbelt HE, Geertzen JH, Jonkman MF, Dijkstra PU. Determinants of Skin Problems of the Stump in Lower-Limb Amputees. Arch Phys Med Rehabil [Internet]. 2009;90(1):74–81. Available from: http://dx.doi.org/10.1016/j.apmr.2008.07.015

[9] Dudek NL, Marks MB, Marshall SC, Chardon JP. Dermatologic conditions associated with use of a lower-extremity prosthesis. Arch Phys Med Rehabil [Internet]. 2005 Apr;86(4):659–63. Available from: https://linkinghub.elsevier.com/retrieve/pii/S0003999304012389

[10] Maciver M, Dixon D, Powell D. Quality of life in young people with limb loss: a systematic review. Disabil Rehabil [Internet]. 2023;0(0):1–12. Available from: https://doi.org/10.1080/09638288.2023.2270908

[11] Safari R. Lower limb prosthetic interfaces: Clinical and technological advancement and potential future direction. Prosthet Orthot Int. 2020;44(6):384–401.

[12] Paternò L, Ibrahimi M, Gruppioni E, Menciassi A, Ricotti L. Sockets for limb prostheses: A review of existing technologies and open challenges. IEEE Trans Biomed Eng. 2018;65(9):1996–2010.

[13] Brånemark R, Brånemark PI, Rydevik B, Myers RR. Osseointegration in skeletal reconstruction and rehabilitation: A review. J Rehabil Res Dev. 2001;38(2):175–81.

[14] Li Y, Brånemark R. Osseointegrierte Prothesen zur Rehabilitation nach Amputation: Das wegweisende schwedische Modell. Unfallchirurg. 2017;120(4):285–92.

[15] Thesleff A, Brånemark R, Håkansson B, Ortiz-Catalan M. Biomechanical Characterisation of Bone-anchored Implant Systems for Amputation Limb Prostheses: A Systematic Review. Ann Biomed Eng [Internet]. 2018 Mar 11;46(3):377–91. Available from: http://link.springer.com/10.1007/s10439-017-1976-4

[16] Frossard L, Ferrada L, Quincey T, Berg D. Cost-effectiveness of transtibial bone-anchored prostheses using osseointegrated fixation: From challenges to preliminary data. J Prosthetics Orthot. 2021;33(3):184–95.

[17] Stenlund P, Trobos M, Lausmaa J, Brånemark R, Thomsen P, Palmquist A. Effect of load on the bone around bone-anchored amputation prostheses. J Orthop Res. 2017;35(5):1113–22.

[18] Palmquist A, Windahl SH, Norlindh B, Brånemark R, Thomsen P. Retrieved bone-anchored percutaneous amputation prosthesis showing maintained osseointegration after 11 years - A case report. Acta Orthop. 2014;85(4):442–5.

[19] Kramer MJ, Tanner BJ, Horvai AE, O'Donnell RJ. Compressive osseointegration promotes viable bone at the endoprosthetic interface: Retrieval study of Compress® implants. Int Orthop. 2008;32(5):567–71.

[20] Nebergall A, Bragdon C, Antonellis A, Kärrholm J, Brånemark R, Malchau H. Stable fixation of an osseointegated implant system for above-the-knee amputees: Titel RSA and radiographic evaluation of migration and bone remodeling in 55 cases. Acta Orthop. 2012;83(2):121–8.

[21] Prochor P, Frossard L, Sajewicz E. Effect of the material's stiffness on stress-shielding in osseointegrated implants for bone-anchored prostheses: A numerical analysis and initial benchmark data. Acta Bioeng Biomech. 2020;22(2).

[22] Savio D, Bagno A. When the Total Hip Replacement Fails : A Review on the. Processes. 2022;10:1–17.

[23] Atallah R, Li JJ, Lu W, Leijendekkers R, Muderis M Al. Osseointegrated Transtibial Implants in Patients with Peripheral Vascular Disease. J Bone Jt Surg. 2017;99(18):1516–23.

[24] Thouvenin C, Bertrand-Marchand M, Klotz R, Puges M, Fabre T, Delgove A. Bone-anchored prostheses for lower limb amputation in a French cohort with 1–15 years of follow-up: implant survival rates, mechanical complications, and reported outcomes. Eur J Orthop Surg Traumatol [Internet]. 2024;34(2):885–92. Available from: https://doi.org/10.1007/s00590-023-03738-0

[25] Lu W, Al Muderis M. The Use of Osseointegrated Titanium Implants to Treat Trans-Tibial Amputees. Arch Phys Med Rehabil [Internet]. 2018;99(10):e106. Available from: https://doi.org/10.1016/j.apmr.2018.07.380

[26] Atallah R, Li JJ, Lu W, Leijendekkers R, Frölke JP, Al Muderis M. Osseointegrated Transtibial Implants in Patients with Peripheral Vascular Disease. J Bone Jt Surg [Internet]. 2017 Sep 20;99(18):1516–23. Available from: https://journals.lww.com/00004623-201709200-00003

[27] Atallah R, Leijendekkers RA, Hoogeboom TJ, Frölke JP. Complications of bone-anchored prostheses for individuals with an extremity amputation: A systematic review. McKinley TO, editor. PLoS One [Internet]. 2018 Aug 9;13(8):e0201821. Available from: https://dx.plos.org/10.1371/journal.pone.0201821

[28] Webster JB, Chou T, Kenly M, English M, Roberts TL, Bloebaum RD. Perceptions and acceptance of osseointegration among individuals with lower limb amputations: A prospective survey study. J Prosthetics Orthot. 2009;21(4):215–22.

[29] Hobara H, Baum BS, Kwon H-J, Linberg A, Wolf EJ, Miller RH, et al. Amputee locomotion: Lower extremity loading using running-specific prostheses. Gait Posture [Internet]. 2014 Jan;39(1):386–90. Available from: https://linkinghub.elsevier.com/retrieve/pii/S0966636213004657

[30] Thesleff A, Ludvigsson S, Ohr E, Ortiz-Catalan M. Load exposure of osseointegrated implants for transfemoral limb prosthesis during running. Proc Annu Int Conf IEEE Eng Med Biol Soc EMBS. 2018;2018-July:1743–6.

[31] D'Angeli V, Belvedere C, Ortolani M, Giannini S, Leardini A. Load along the tibial shaft during activities of daily living. J Biomech [Internet]. 2014;47(5):1198–205. Available from: http://dx.doi.org/10.1016/j.jbiomech.2014.01.045

[32] Wehner T, Claes L, Simon U. Internal loads in the human tibia during gait. Clin Biomech [Internet]. 2009;24(3):299–302. Available from: http://dx.doi.org/10.1016/j.clinbiomech.2008.12.007

[33] Galteri G, Cristofolini L. In vitro and in silico methods for the biomechanical assessment of osseointegrated transfemoral prostheses: a systematic review. Front Bioeng Biotechnol [Internet]. 2023 Aug 17;11(August). Available from: https://www.frontiersin.org/articles/10.3389/fbioe.2023.1237919/full

[34] Ahmed K, Greene RJ, Aston W, Briggs T, Pendegrass C, Moazen M, et al. Experimental Validation of an ITAP Numerical Model and the Effect of Implant Stem Stiffness on Bone Strain Energy. Ann Biomed Eng. 2020;48(4):1382–95.

[35] Tomaszewski PK, Lasnier B, Hannink G, Verkerke GJ, Verdonschot N. Experimental assessment of a new direct fixation implant for artificial limbs. J Mech Behav Biomed Mater [Internet]. 2013;21:77–85. Available from: http://dx.doi.org/10.1016/j.jmbbm.2013.02.012

[36] Leijendekkers RA, van Hinte G, Frölke JP, van de Meent H, Nijhuis-van der Sanden MWG, Staal JB. Comparison of bone-anchored prostheses and socket prostheses for patients with a lower extremity amputation: a systematic review. Disabil Rehabil. 2017;39(11):1045–58.

[37] Klineberg I, Calford MB, Dreher B, Henry P, Macefield V, Miles T, et al. A consensus statement on osseoperception. Clin Exp Pharmacol Physiol. 2005;32(1–2):145–6.

[38] Frossard LA, Tranberg R, Haggstrom E, Pearcy M, Brnemark R. Load on osseointegrated fixation of a transfemoral amputee during a fall: Loading, descent, impact and recovery analysis. Prosthet Orthot Int. 2010;34(1):85–97.

[39] Sartori M, Maculan M, Pizzolato C, Reggiani M, Farina D. Modeling and simulating the neuromuscular mechanisms regulating ankle and knee joint stiffness during human locomotion. J Neurophysiol. 2015;114(4):2509–27.

[40] Sepp LA, Baum BS, Nelson-Wong E, Silverman AK. Joint work and ground reaction forces during running with daily-use and running-specific prostheses. J Biomech [Internet]. 2020 Mar;101:109629. Available from: https://doi.org/10.1016/j.jbiomech.2020.109629

[41] Groothuis A, Houdijk H. The Effect of Prosthetic Alignment on Prosthetic and Total Leg Stiffness While Running With Simulated Running-Specific Prostheses. Front Sport Act Living. 2019;1(August):1–10.

[42] Vicon. Lower body kinematics—Nexus 2.12 Documentation; 2023. [Internet]. Available from: https://docs.vicon.com/display/ Nexus212/Lower+body+kinematics.

[43] Jonkergouw N, Prins MR, van der Wurff P, Gijsbers J, Houdijk H, Buis AWP. Dynamic alignment using external socket reaction moments in trans-tibial amputees. Gait Posture [Internet]. 2019;68:122–9. Available from: https://www.sciencedirect.com/science/article/pii/S0966636218305666

[44] Hof AL. TECHNICAL NOTE AN EXPLICIT EXPRESSION FOR THE MOMENT IN MULTIBODY

SYSTEMS. J Biomech. 1992;25(10):1209–11.

[45] Kingma I, Toussaint HM, De Looze MP, Van Dieen JH. Segment inertial parameter evaluation in two anthropometric models by application of a dynamic linked segment model. J Biomech [Internet]. 1996 May;29(5):693–704. Available from: https://www.sciencedirect.com/science/article/pii/0021929095000860?via%3Dihub

[46] de Leva P. Adjustments to Zatsiorsky-Seluyanov's segment inertia parameters. J Biomech [Internet]. 1996;29(9):1223–30. Available from: https://www.sciencedirect.com/science/article/pii/0021929095001786

[47] Besier TF, Lloyd DG, Cochrane JL, Ackland TR. External loading of the knee joint during running and cutting maneuvers. Med Sci Sports Exerc. 2001;33(7):1168–75.

[48] Frossard L. Loading characteristics data applied on osseointegrated implant by transfemoral bone-anchored prostheses fitted with basic components during daily activities. Data Br [Internet]. 2019;26:104492. Available from: https://doi.org/10.1016/j.dib.2019.104492

[49] Koehler SR, Dhaher YY, Hansen AH. Cross-validation of a portable, six-degree-of-freedom load cell for use in lower-limb prosthetics research. J Biomech [Internet]. 2014;47(6):1542–7. Available from: http://dx.doi.org/10.1016/j.jbiomech.2014.01.048

[50] Brånemark R, Brånemark PI, Rydevik B, Myers RR. Osseointegration in skeletal reconstruction and rehabilitation: a review. J Rehabil Res Dev [Internet]. 2001;38(2):175–81. Available from: http://www.ncbi.nlm.nih.gov/pubmed/11392650

[51] Brånemark R, Emanuelsson L, Palmquist A, Thomsen P. Bone response to laser-induced micro- and nano-size titanium surface features. Nanomedicine Nanotechnology, Biol Med [Internet]. 2011;7(2):220–7. Available from: https://www.sciencedirect.com/science/article/pii/S1549963410003576

[52] Aschoff HH, Juhnke DL. Endo-Exo-Prothesen: Osseointegrierte, perkutan ausgeleitete Implantate zur Rehabilitation nach Gliedmaßenamputation. Unfallchirurg. 2016;119(5):421–7.

[53] Los M. Implant load during running on a transtibial bone anchored prosthesis, a multibody modelling experimental approach. 2024;

[54] Fedorov A, Beichel R, Kalpathy-Cramer J, Finet J, Fillion-Robin J-C, Pujol S, et al. 3D Slicer as an image computing platform for the Quantitative Imaging Network. Magn Reson Imaging [Internet]. 2012 Nov;30(9):1323–41. Available from: https://linkinghub.elsevier.com/retrieve/pii/S0730725X12001816

[55] Keyak JH, Kaneko TS, Tehranzadeh J, Skinner HB. Predicting proximal femoral strength using structural engineering models. Clin Orthop Relat Res. 2005;437(437):219–28.

[56] Eggermont F, Verdonschot N, van der Linden Y, Tanck E. Calibration with or without phantom for fracture risk prediction in cancer patients with femoral bone metastases using CT-based finite element models. Pérez MA, editor. PLoS One [Internet]. 2019 Jul 30;14(7):e0220564. Available from: https://dx.plos.org/10.1371/journal.pone.0220564

[57] Renishaw. Data sheet: RenAM 500 series Titanium Ti6Al4V (Grade 23) material data sheet [Internet]. 2023 [cited 2024 Apr 3]. Available from: https://www.renishaw.com/resourcecentre/en/details/RenAM-500-series-Titanium-Ti6Al4V-Grade-23-material-data-sheet--130336?lang=en

[58] Wally ZJ, van Grunsven W, Claeyssens F, Goodall R, Reilly GC. Porous titanium for dental implant applications. Metals (Basel). 2015;5(4):1902–20.

[59] Biewener AA. Calcified Tissue Safety Factors in Bone Strength. Flying. 1993;53:68–74.

[60] Willie BM, Zimmermann EA, Vitienes I, Main RP, Komarova S V. Bone adaptation: Safety factors and load predictability in shaping skeletal form. Bone [Internet]. 2020;131(July 2019):115114. Available from: https://doi.org/10.1016/j.bone.2019.115114

[61] Kenkre JS, Bassett JHD. The bone remodelling cycle. Ann Clin Biochem. 2018;55(3):308–27.

[62] Haket LM, Frölke JPM, Verdonschot N, Tomaszewski PK, van de Meent H. Periprosthetic cortical bone remodeling in patients with an osseointegrated leg prosthesis. J Orthop Res. 2017;35(6):1237–41.

[63] Wankier Z, Taylor C, Drew A, Kubiak E, Agarwal J, Sinclair S. Use of computer tomography imaging for analyzing bone remodeling around a percutaneous osseointegrated implant. J Orthop Res. 2022;40(9):2065–75.

[64] Frost HM. A 2003 update of bone physiology and Wolff s law for clinicians. Angle Orthod. 2004;74(1):3–15.

[65] Tsubota K ichi, Suzuki Y, Yamada T, Hojo M, Makinouchi A, Adachi T. Computer simulation of trabecular remodeling in human proximal femur using large-scale voxel FE models: Approach to understanding Wolff's law. J Biomech. 2009;42(8):1088–94.

[66] Jones MD, Buckle CL. How does aseptic loosening occur and how can we prevent it? Orthop Trauma [Internet]. 2020;34(3):146–52. Available from: https://doi.org/10.1016/j.mporth.2020.03.008

[67] Chong DYR, Hansen UN, Amis AA. Analysis of bone-prosthesis interface micromotion for cementless tibial prosthesis fixation and the influence of loading conditions. J Biomech [Internet]. 2010;43(6):1074–80. Available from: http://dx.doi.org/10.1016/j.jbiomech.2009.12.006

[68] Azadi M, Farzannasab M. Evaluation of high-cycle fatigue behavior in compact bones at different loading frequencies. Meccanica [Internet]. 2018;53(14):3517–26. Available from: https://doi.org/10.1007/s11012-018-0893-4

[69] Van Rietbergen B, Huiskes R, Weinans H, Sumner DR, Turner TM, Galante JO. The mechanism of bone remodeling and resorption around press-fitted THA stems. J Biomech. 1993;26(4–5):369–82.

Appendix A – Von Mises stress in transverse cross-sections of the tibia

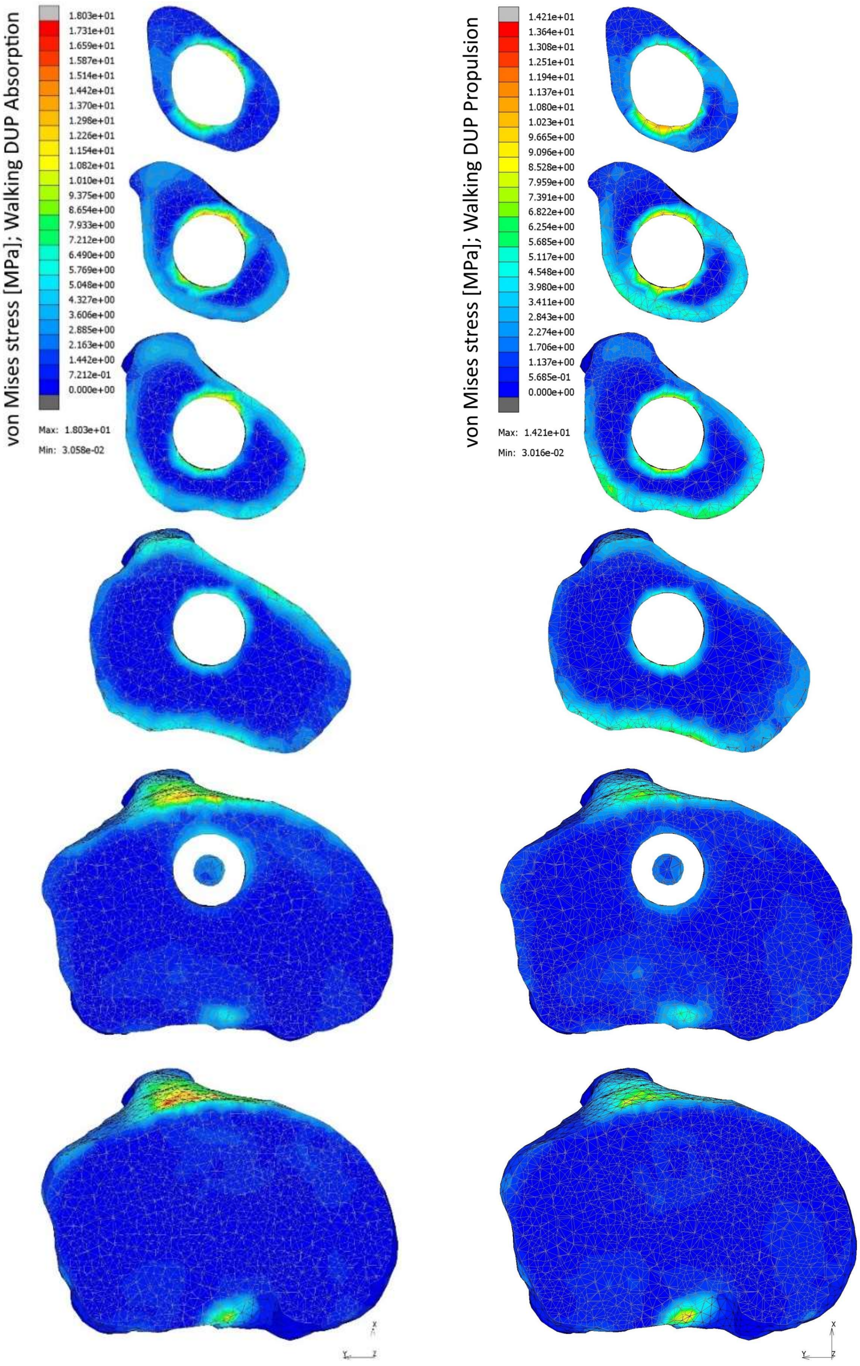

Figure 23 Von Mises stress of walking for absorption (left) and propulsion (right) load cases presented in transverse cross sections of the tibia at +10, +25, +40, +55, +70, +75mm offset from the distal tip. Scales are not uniform to illustrate the distribution for each load case separately.

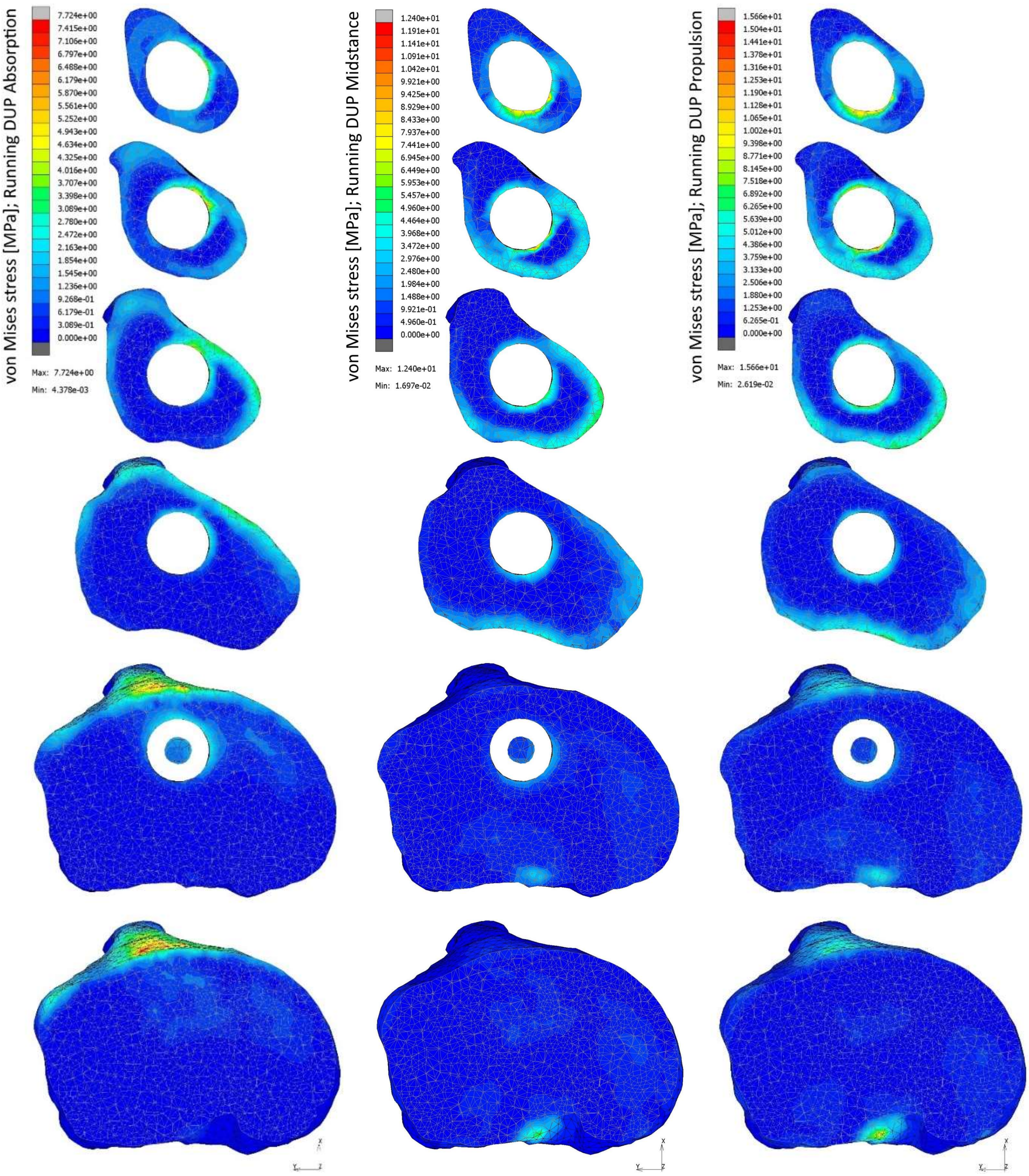

Figure 24 Von Mises stress of running on a DUP for absorption (left), midstance (middle) and propulsion (right) load cases presented in transverse cross sections of the tibia at +10, +25, +40, +55, +70, +75mm offset from the distal tip. Scales are not uniform to illustrate the distribution for each load case separately.

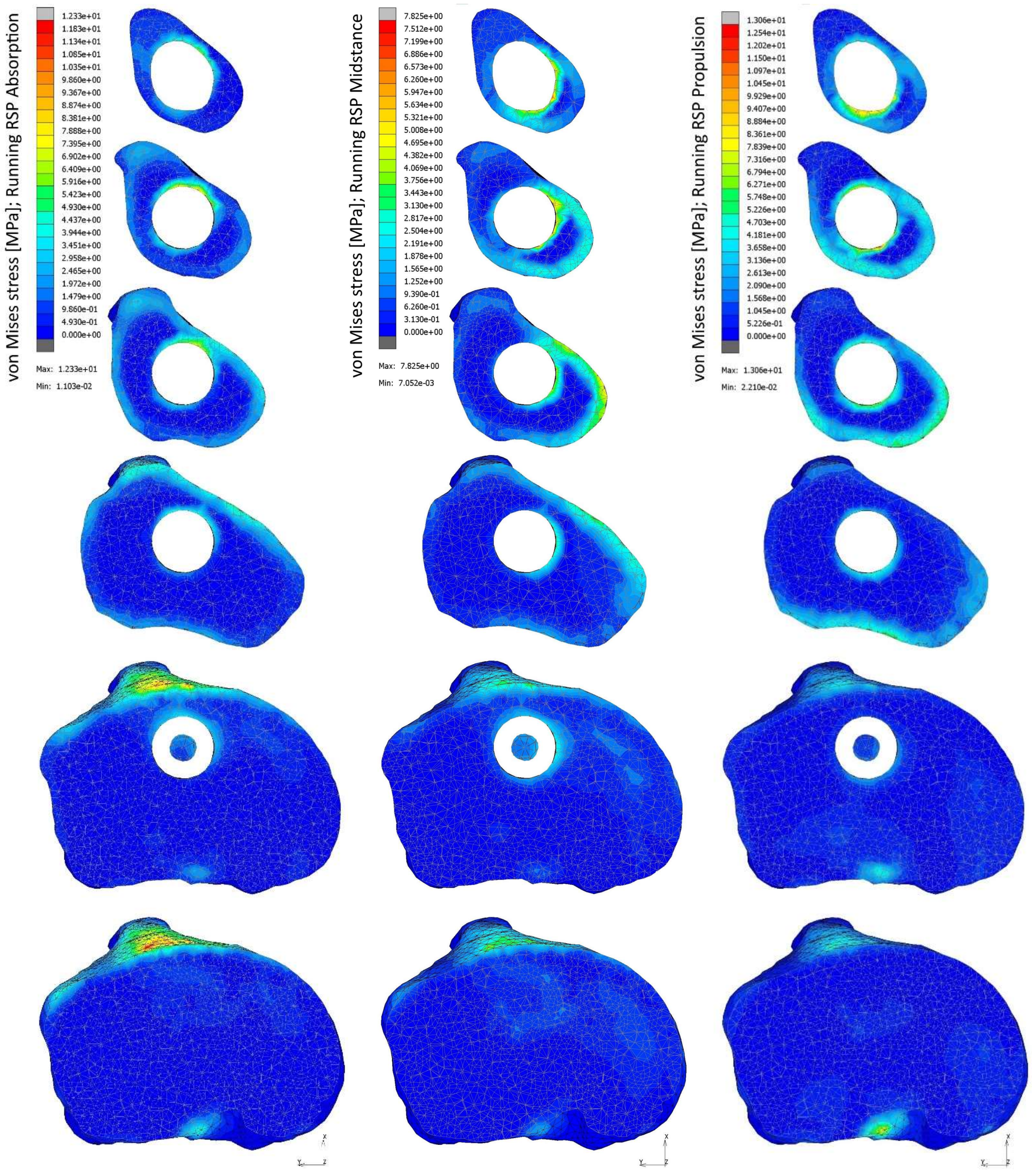

Figure 25 Von Mises stress of running on a RSP for absorption (left), midstance (middle) and propulsion (right) load cases presented in transverse cross sections of the tibia at +10, +25, +40, +55, +70, +75mm offset from the distal tip. Scales are not uniform to illustrate the distribution for each load case separately.

Appendix B – Von Mises Stress/strength ratio in transverse cross-sections of the tibia

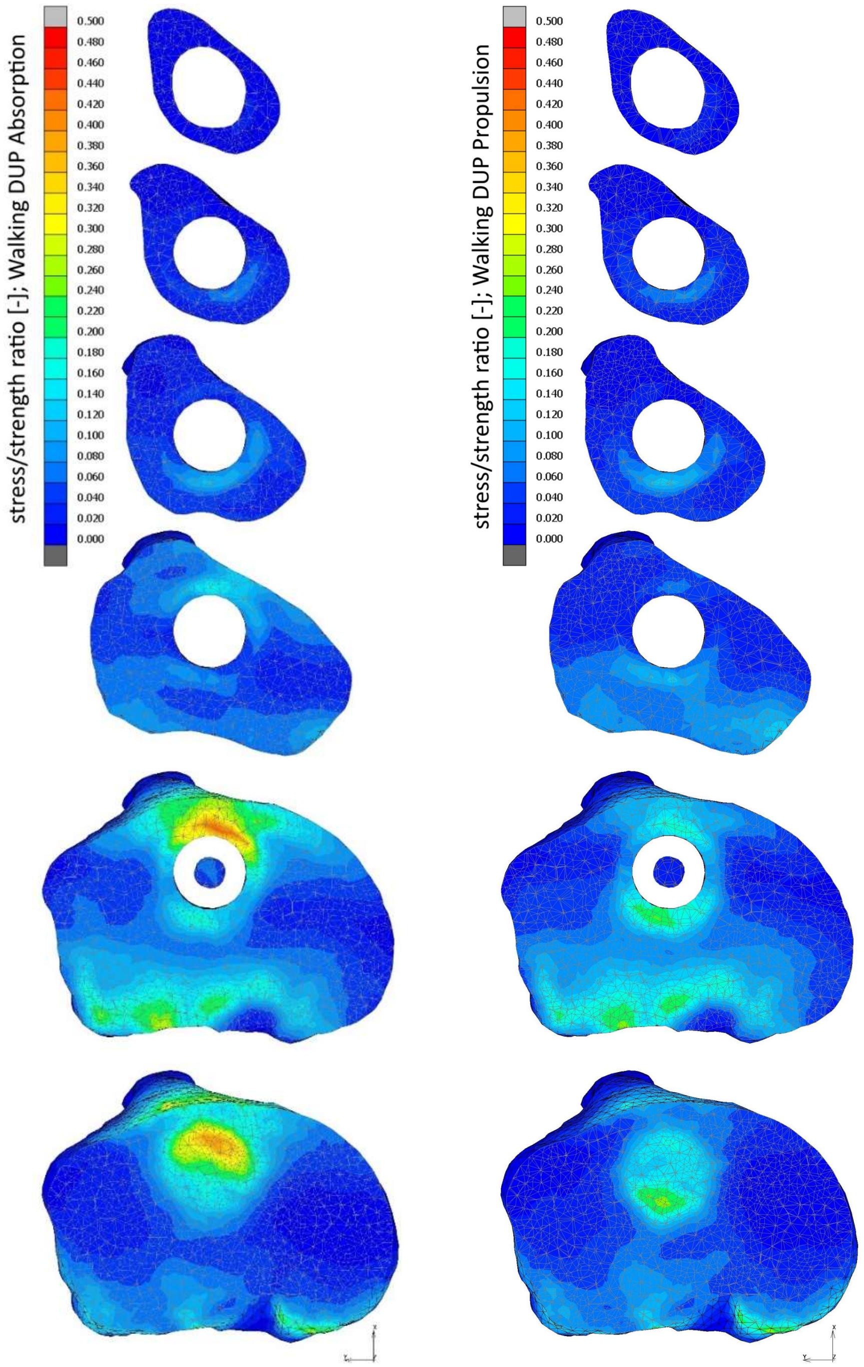

Figure 26 Stress/strength ratio of walking on a DUP for absorption (left), midstance (middle) and propulsion (right) load cases presented in transverse cross sections of the tibia at +10, +25, +40, +55, +70, +75mm offset from the distal tip. Uniform colour scale ranging from 0 to 0.5 is used for all figures presenting the ratio.

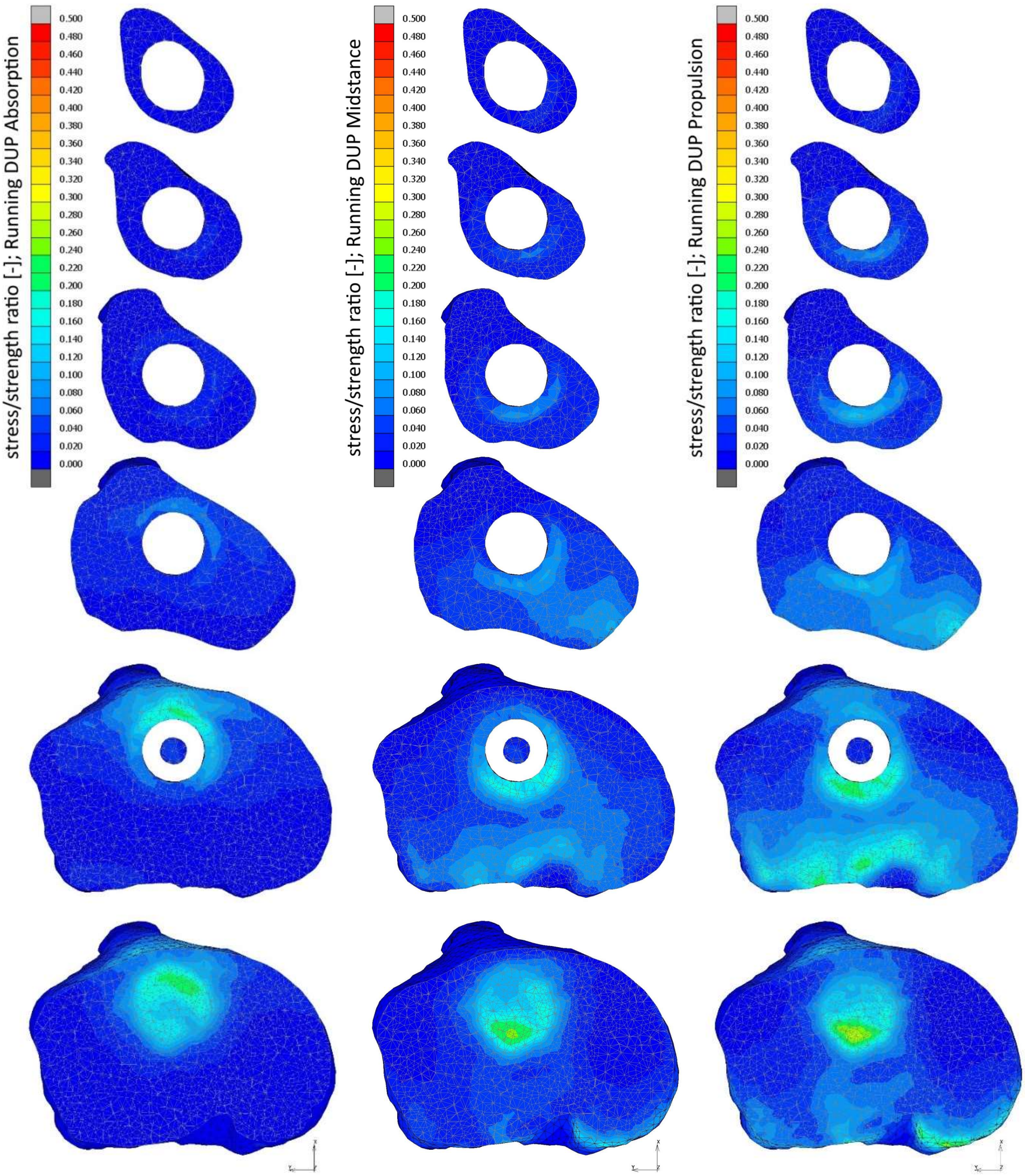

Figure 27 Stress/strength ratio of running on a DUP for absorption (left), midstance (middle) and propulsion (right) load cases presented in transverse cross sections of the tibia at +10, +25, +40, +55, +70, +75mm offset from the distal tip. Uniform colour scale ranging from 0 to 0.5 is used for all figures presenting the ratio.

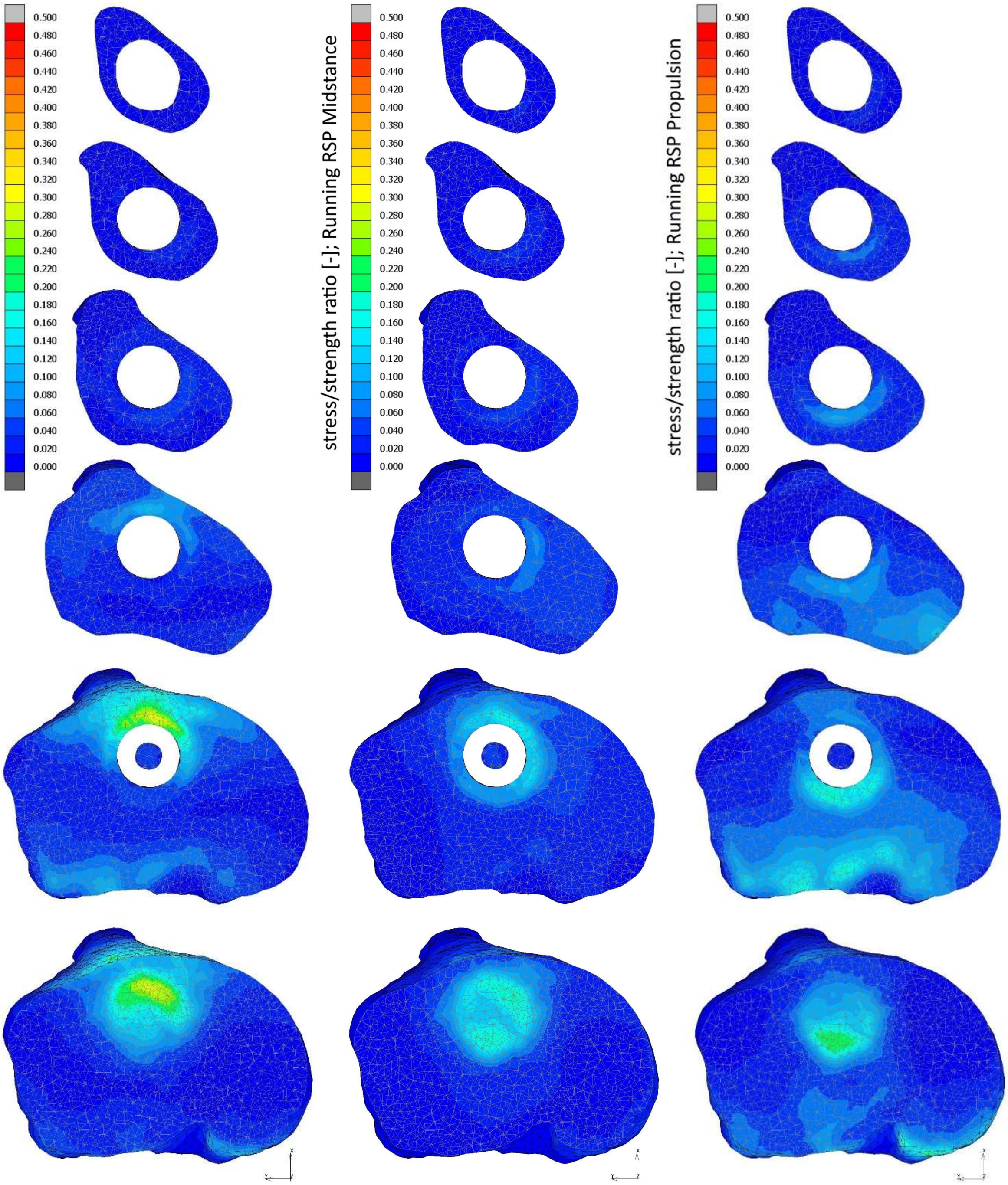

Figure 28 Stress/strength ratio of running on a RSP for absorption (left), midstance (middle) and propulsion (right) load cases presented in transverse cross sections of the tibia at +10, +25, +40, +55, +70, +75mm offset from the distal tip. Uniform colour scale ranging from 0 to 0.5 is used for all figures presenting the ratio.